Article

SOURCE DATA | TRANSPARENT PROCESS | OPEN ACCESS

THE EMBO JOURNAL

SIRT7 activates quiescent hair follicle stem cells to ensure hair growth in mice

Guo Li[1,†], Xiaolong Tang[2,3,†], Shuping Zhang[1], Meiling Jin[4], Ming Wang[2,3], Zhili Deng[1], Zuojun Liu[2,3], Minxian Qian[2,3], Wei Shi[1], Zimei Wang[2,3], Hongfu Xie[1], Ji Li[1,5,6,7,*] & Baohua Liu[2,3,8,**]

Abstract

Hair follicle stem cells (HFSCs) are maintained in a quiescent state until activated to grow, but the mechanisms that reactivate the quiescent HFSC reservoir are unclear. Here, we find that loss of *Sirt7* in mice impedes hair follicle life-cycle transition from telogen to anagen phase, resulting in delay of hair growth. Conversely, *Sirt7* overexpression during telogen phase facilitated HSFC anagen entry and accelerated hair growth. Mechanistically, *Sirt7* is upregulated in HFSCs during the telogen-to-anagen transition, and HFSC-specific *Sirt7* knockout mice (*Sirt7*$^{f/f}$;K15-Cre) exhibit a similar hair growth delay. At the molecular level, Sirt7 interacts with and deacetylates the transcriptional regulator Nfatc1 at K612, causing PA28γ-dependent proteasomal degradation to terminate Nfatc1-mediated telogen quiescence and boost anagen entry. Cyclosporin A, a potent calcineurin inhibitor, suppresses nuclear retention of Nfatc1, abrogates hair follicle cycle delay, and promotes hair growth in *Sirt7*$^{-/-}$ mice. Furthermore, *Sirt7* is downregulated in aged HFSCs, and exogenous *Sirt7* overexpression promotes hair growth in aged animals. These data reveal that Sirt7 activates HFSCs by destabilizing Nfatc1 to ensure hair follicle cycle initiation.

Keywords aging; hair follicle stem cells; Nfatc1; PA28γ; Sirt7
Subject Categories Stem Cells & Regenerative Medicine; Skin
DOI 10.15252/embj.2019104365 | Received 27 December 2019 | Revised 11 June 2020 | Accepted 14 June 2020 | Published online 21 July 2020
The EMBO Journal (2020) 39: e104365

See also: **M Simon *et al*** (September 2020)

Introduction

Hair follicles (HFs) build up within 2 weeks after birth in mice to produce what is considered a "mini-organ" in the skin (Stenn & Paus, 2001). HFs undergo many growth–rest cycles over time; these cycles comprise anagen (growth), catagen (regression), and telogen (rest) phases that are driven by HF stem cells (HFSCs) (Millar, 2002; Schmidt-Ullrich & Paus, 2005; Rishikaysh *et al*, 2014). These stem cells are found within the HF outer root sheath (ORS), or "bulge" (Cotsarelis *et al*, 1990). A complex molecular cascade accompanies HF transition, comprising inhibited BMP and activated Shh and Wnt/β-catenin/Lef-1 signaling (Sato *et al*, 1999; Botchkarev *et al*, 2001; Huelsken *et al*, 2001; Reddy *et al*, 2001). The BMP signal maintains HFs in the telogen phase (Blanpain *et al*, 2004). If BMP is antagonized by an inhibitory signal, such as *de novo* Noggin expression (Botchkarev *et al*, 2001), a new HF cycle is initiated that coincides with the telogen-to-anagen transition. Here, Shh signaling activates the Wnt/β-catenin/Lef-1pathway, which boosts cell proliferation and hair shaft formation (Botchkarev *et al*, 2002; Alonso & Fuchs, 2003; Andl *et al*, 2004; Zhang *et al*, 2006). During the anagen-to-catagen transition, TGF-β1 signaling promotes HF degeneration by arresting keratinocyte proliferation arrest and inducing apoptosis. The HF then returns to a quiescent state (Foitzik *et al*, 2000; Botchkarev & Kishimoto, 2003).

Hair thinning and loss are prominent characteristics of aging. These features are largely attributable to HFSC reservoir depletion, functional decline, and extended dormancy (Lei & Chuong, 2016). In aged mice, HFSCs usually fail or delay to start a new hair cycle owing to an imbalance between quiescence and activation signaling in HFs. Numerous transcription factors, including Sox9, Tbx1, Lhx2, TCF3/4, Foxc1 and Nfatc1, help maintain a quiescent and undifferentiated HFSC status (Blanpain *et al*, 2004; Tumbar *et al*, 2004; Horsley *et al*,

1 Department of Dermatology, Xiangya Hospital, Central South University, Changsha, China
2 Shenzhen Key Laboratory for Systemic Aging and Intervention (SAI), National Engineering Research Center for Biotechnology (Shenzhen), International Cancer Center, Shenzhen University, Shenzhen, China
3 Guangdong Key Laboratory of Genome Stability and Human Disease Prevention, Department of Biochemistry & Molecular Biology, School of Basic Medical Sciences, Shenzhen University, Shenzhen, China
4 CAS Key Laboratory of Quantitative Engineering Biology, Shenzhen Institute of Synthetic Biology, Shenzhen Institutes of Advanced Technology, Chinese Academy of Sciences, Shenzhen, China
5 National Clinical Research Center for Geriatric Disorders, Xiangya Hospital, Central South University, Changsha, Hunan, China
6 Key Laboratory of Organ Injury, Aging and Regenerative Medicine of Hunan Province, Changsha, Hunan, China
7 Department of Dermatology, The Second Affiliated Hospital of Xinjiang Medical University, Urumqi, China
8 Guangdong Provincial Key Laboratory of Regional Immunity and Diseases, School of Basic Medical Sciences, Shenzhen University Health Science Center, Shenzhen, China
*Corresponding author. Tel: +86 731 89753799; E-mail: liji_xy@csu.edu.cn
**Corresponding author. Tel: +86 755 86674609; E-mail: ppliew@szu.edu.cn
†Those authors contributed equally to this work

2008). For example, *Foxc1* deletion compromises quiescence by suppressing BMP and Nfatc1 signaling; this effect causes premature HFSC activation (Lay *et al*, 2016; Wang *et al*, 2016). NFATc1 is essential for HFSC quiescence (Horsley *et al*, 2008): During aging, hyper-accumulation of nuclear Nfatc1 extends the dormant period of HFSCs (Keyes *et al*, 2013). The precise mechanisms governing NFATc1 dynamics in normal adult hair cycling and aging, however, are poorly understood. Understanding the mechanisms that evoke quiescent HFSCs is equally important to help treat or prevent age-associated hair thinning and loss.

The sirtuin protein family is involved in regulating longevity (Wu *et al*, 2018). Data from phenotypic analyses of knockout mice suggest that *Sirt1*, *Sirt6,* and *Sirt7* are potential longevity-associated genes (Vakhrusheva *et al*, 2008; Kawahara *et al*, 2009; Kanfi *et al*, 2012; Satoh *et al*, 2013; Vazquez *et al*, 2016). Sirt7 is an NAD^+-dependent deacylase and its expression declines in senescent cells (Blank & Grummt, 2017; Wu *et al*, 2018). Many studies have uncovered links between Sirt7 and aging: $Sirt7^{-/-}$ mice have a shortened lifespan by up to 50% and exhibit multiple aging phenotypes, including hepatic steatosis, gonadal fat pad content depletion, cardiac hypertrophy, and hematopoietic stem cell reduction (Shin *et al*, 2013; Ryu *et al*, 2014; Yoshizawa *et al*, 2014; Araki *et al*, 2015; Mohrin *et al*, 2015; Tang, 2015; Vazquez *et al*, 2016; Tang *et al*, 2019). Here, using genetically modified mice, we aimed to explore the role of Sirt7 in HFSCs and hair loss with aging.

Results

Loss of *Sirt7* delays telogen-to-anagen transition in murine HFs

Loss of *Sirt7* accelerates aging in mice (Vazquez *et al*, 2016). Hair dysfunction is a common characteristic in the elderly. Remarkably, we observed a notable decrease in Sirt7 expression in hair follicles (HFs) in aged mice (18 months) compared to that of young mice (3 months). By contrast, Sirt1 and Sirt6 exhibited only a marginal change in expression level (Appendix Fig S1A). We thus focused our attention on Sirt7. First, to examine the role of *Sirt7* in aging-related hair regeneration, we generated whole-body *Sirt7* knockout (KO) mice. Immunohistochemical (IHC) staining and Western blotting confirmed that Sirt7 was expressed in $Sirt7^{+/+}$ HFs (skin) but was absent in $Sirt7^{-/-}$ HFs (skin) (Appendix Fig S1B and C). $Sirt7^{-/-}$ and $Sirt7^{+/+}$ mice showed only a marginal difference in the first postnatal hair cycle (postnatal days P6, P10, P14, to P20), with comparable levels of hair growth and color (Appendix Fig S1D and E). This finding indicates that the initial HF morphogenesis *per se* is not affected by *Sirt7* loss.

To assess whether Sirt7 regulates adult hair growth, we shaved the hair coat of female $Sirt7^{+/+}$ and $Sirt7^{-/-}$ mice on postnatal day (P) 60, when the HFs of both genotypes were in the second telogen phase (Fig 1A). We evaluated hair coat recovery based on skin pigmentation and hair shaft growth as described (Stenn & Paus, 2001; Chai *et al*, 2019). By P120, $Sirt7^{+/+}$ mice recovered an almost full hair coat, while the $Sirt7^{-/-}$ mice showed only ~ 25% recovery (Fig 1A and B). In parallel, hematoxylin and eosin (H&E) staining of the unshaved skin showed that at P90, a large population of $Sirt7^{+/+}$ HFs had developed to a full size, indicating the entry of anagen phase, while $Sirt7^{-/-}$ HFs remained in telogen phase (Fig 1C, left). By the time, the $Sirt7^{-/-}$ HFs had progressed into mid-anagen phase, and at around P130, the $Sirt7^{+/+}$ HFs had already moved to the next telogen phase (Fig 1C, right). Once they enter anagen phase, P-cadherin$^+$ cells in the hair germ (HG) respond to growth signals and become proliferative, as indicated by Ki67 expression (Horsley *et al*, 2008). Consistently, we observed high Ki67 expression at P74 (early anagen) in $Sirt7^{+/+}$ HGs, but low-to-no Ki67 in $Sirt7^{-/-}$ HFs even at P90 (Fig 1D and E).

To confirm our findings, we generated a well-described depilation model to induce homogenous and synchronized HF cycling (Plasari *et al*, 2010). Seven days after depilation, the dorsal skin of $Sirt7^{+/+}$ mice showed deep pigmentation, indicating anagen entry, while that of $Sirt7^{-/-}$ mice remained pink, indicative of telogen phase (Appendix Fig S1F). Indeed, $Sirt7^{-/-}$ mice showed an extended telogen phase by almost 30 days (Fig 1F). Together, these data suggest that loss of *Sirt7* delays the telogen-to-anagen transition in murine HFs.

Induced *Sirt7* expression shortens telogen phase and facilitates anagen entry

We next asked whether forced *Sirt7* expression in HFs in telogen phase would promote anagen entry. We used an inducible *Sirt7* transgenic mouse line (*Sirt7*-TG) (Tang *et al*, 2017), in which *Sirt7* expression could be induced by doxycycline (Dox) at the desired time. *Sirt7*-TG and wild-type (WT) littermate control mice were exposed to Dox (2 mg/ml, dissolved in water) at P42, when the HFs of both genotypes were both in telogen phase. We first confirmed Sirt7 overexpression by IHC staining at P56 (Appendix Fig S1G). Then, we examined hair coat recovery after shaving the telogen dorsal hair at P45. Strikingly, by P100, *Sirt7*-TG mice had recovered an almost full hair coat, while their WT littermates recovered only up to 50% hair (Fig 1G and H). Consistently, *Sirt7*-TG HGs showed prominent Ki67 expression by P65 (Fig 1I and J), significantly ahead of Ki67 expression in WT HGs, which was detectable from P74. Morphological analysis of the unshaved dorsal skin also suggested early anagen entry of *Sirt7*-TG HFs compared to WT HFs (Fig 1K). Thus, forced *Sirt7* overexpression shortened the HF telogen phase by almost 20 days compared to WT mice (Fig 1L). Taken together, we detected an unaltered first hair cycle but an altered second hair cycle in our *Sirt7* mutants: $Sirt7^{-/-}$ mice showed an extended telogen phase and *Sirt7*-TG mice showed a shortened telogen phase (Fig 1M).

Sirt7 deletion delays HFSC activation

HFSCs reside in the HF bulge: During hair regeneration in adulthood, these HFSCs undergo sequential activation and quiescence. HF cycling is regulated by the amount of dynamic signals (Hsu *et al*, 2011). We noted that a burst of Sirt7 expression first appeared in the HFSCs residing in the late telogen bulge. The expression levels progressively increased during the telogen-to-anagen shift in $Sirt7^{+/+}$ HFs, regardless of normal hair cycling or induction by depilation (Fig 2A and B, and Appendix Fig S2A). By contrast, Sirt7 levels remained constant in the interfollicular epidermis (IFE) and intradermal white adipose tissue (dWAT), and almost comparable in the sebaceous gland (SG) (Appendix Fig S2B–D). Thus, Sirt7 expression in HFSCs was specifically coupled with hair cycling progression. Consistently, anagen bulge HFSCs showed a 2-fold increase in *Sirt7*

expression compared to those telogen bulge HFSCs (Appendix Fig S2E).

Of note, CD34 staining and FACS analysis showed that the number of HFSCs was comparable between *Sirt7*$^{+/+}$ and *Sirt7*$^{-/-}$ mice (Appendix Fig S2F and G). This finding was consistent with our observation of normal HF morphogenesis in *Sirt7*$^{-/-}$ mice and encouraged us to explore whether Sirt7 promotes HFSC activation. To that end, we generated epidermal bulge stem cell-specific *Sirt7*

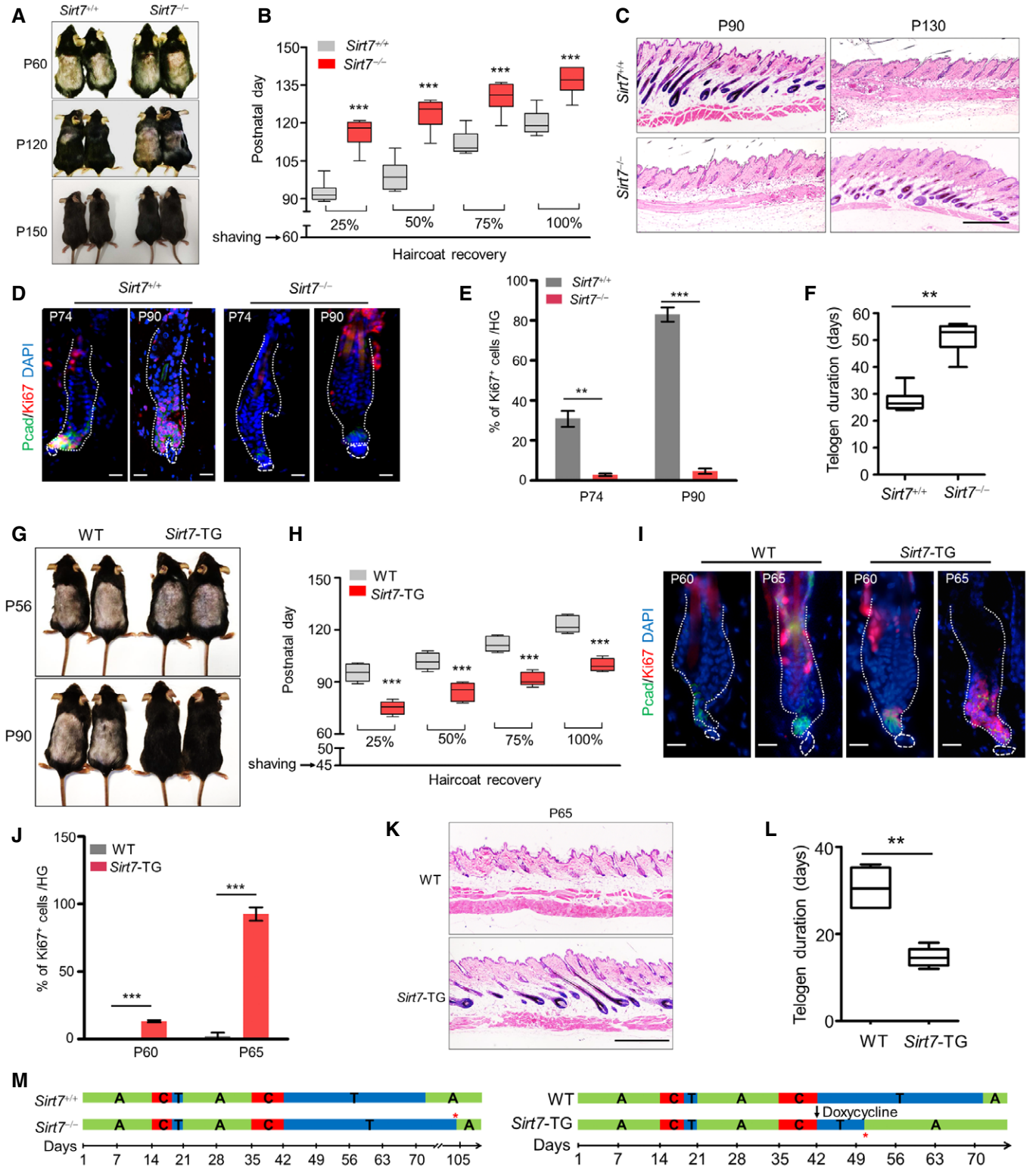

Figure 1.

Figure 1. Sirt7 promotes HF telogen-to-anagen transition.

A The hair coats of *Sirt7*$^{-/-}$ and *Sirt7*$^{+/+}$ mice were clipped on P60 in the mid-second telogen phase. Images were captured at P60, P120, and P150.
B The postnatal day when the hair coat recovered by 25, 50, 75, and 100% in shaved *Sirt7*$^{-/-}$ and *Sirt7*$^{+/+}$ mice. n = 6 mice/genotype. Box-and-whisker plots: mid-line, median; box, 25th and 75th percentiles; whiskers, minimum, and maximum.
C H&E staining of the skin in unshaved *Sirt7*$^{-/-}$ and *Sirt7*$^{+/+}$ mice on P90 and P130.
D Representative immunofluorescence images showing Ki67 and p-cadherin (Pcad, labeling HG cells) expression in *Sirt7*$^{-/-}$ and *Sirt7*$^{+/+}$ HFs on P74 and P90. The HF boundary and dermal papilla (DP) are denoted by the dotted and dashed lines, respectively.
E Percent Ki67-positive cells in each hair germ in D; n = 3 mice and 10 HGs were counted in each mouse.
F Telogen duration in *Sirt7*$^{-/-}$ and *Sirt7*$^{+/+}$ mice. n = 6 mice per genotype. Box-and-whisker plots: mid-line, median; box, 25th and 75th percentiles; whiskers, minimum, and maximum.
G The hair coats of *Sirt7*-TG and WT mice were clipped on P45, and images were captured on P56 and P90.
H The postnatal day when the hair coat recovered by 25, 50, 75, and 100% in shaved *Sirt7*-TG and WT mice. n = 6 mice per genotype. Box-and-whisker plots: mid-line, median; box, 25th and 75th percentiles; whiskers, minimum, and maximum.
I Representative immunofluorescence images showing Ki67 and Pcad expression in *Sirt7*-TG and WT HFs at P60 and P65. The HF boundary and DP are noted by the dotted and dashed lines, respectively.
J The percentage of Ki67-positive cells in each HG; n = 3 mice, and 10 HGs were counted in each mouse.
K H&E staining of skin tissues in unshaved *Sirt7*-TG and WT mice on P65.
L Telogen duration in *Sirt7*-TG and WT mice. n = 6 mice per genotype.Box-and-whisker plots: mid-line, median; box, 25th and 75th percentiles; whiskers, minimum, and maximum.
M Abstracted HF cycling in *Sirt7*$^{-/-}$, *Sirt7*$^{+/+}$, *Sirt7*-TG, and WT mice mentioned above. The red star indicates anagen entry in *Sirt7*$^{-/-}$ and *Sirt7*-TG mice; the black arrows show the date of doxycycline feeding.

Data information: Scale bar, 50 μm for immunofluorescence images; 200 μm for H&E staining images. The data represent the means ± s.e.m. $^{**}P < 0.01$, $^{***}P < 0.001$, determined by Student's t-test.

KO mice (*Sirt7*$^{f/f}$;K15-Cre) by crossing Keratin 15 (K15)-CrePGR (Cre activation induced by mifepristone) mice to *Sirt7* floxed mice (*Sirt7*$^{f/f}$) (Morris *et al*, 2004; Oshimori & Fuchs, 2012). At P42, we treated *Sirt7*$^{f/f}$;K15-Cre mice and *Sirt7*$^{f/f}$ littermates with mifepristone and confirmed *Sirt7* deletion in bulge stem cells by IHC staining at P74 (Appendix Fig S2H). Compared to other organs and tissues, only the skin exhibited prominent *Cre* expression and a significant *Sirt7* reduction by 50%, thus ruling out possible off-target effects (Appendix Fig S2I). Notably, *Sirt7*$^{f/f}$;K15-Cre mice possessed an equivalent number of HFSCs compared to their littermate controls (Appendix Fig S2J).

To assess the impact of *Sirt7* loss in epidermal stem cells on HF cycling, we clipped the dorsal hair of both genotypes at P60 (at terlogen phase, Fig 2C) and monitored the subsequent hair growth. *Sirt7*$^{f/f}$ control mice fully recovered the hair coat by P125, while *Sirt7*$^{f/f}$;K15-Cre mice presented an almost 50% recovery (Fig 2C and D). This extension in telogen phase in *Sirt7*$^{f/f}$;K15-Cre mice was evidenced by H&E and low Ki67 staining in HG and bulge cells in the *Sirt7*$^{f/f}$;K15-Cre skin (Fig 2E–H). Additionally, the HFSC number was comparable between *Sirt7*$^{f/f}$;K15-Cre and *Sirt7*$^{f/f}$ mice (marked by CD34) (Fig 2F, lower panel and Appendix Fig S2K), again implicating that *Sirt7* loss has little impact on HF development but shifts HF cycling (Fig 2I).

To further confirm that Sirt7 contributes to HFSC activation, we conducted a BrdU pulse-chase experiment in *Sirt7*$^{+/+}$ and *Sirt7*$^{-/-}$ mice following depilation-induced hair cycle synchronization at telogen phase. Depilation removes an inner bulge layer of BMP6 and FGF18-expressing cells that consequently activates quiescent HFSCs (Hsu *et al*, 2011). On post-depilation days 2 and 4, we found that much fewer *Sirt7*$^{-/-}$ bulge cells incorporated BrdU, indicating less activation of HFSCs at early anagen phase (Appendix Fig S3A and B). Despite this apparent delay, the number of BrdU-labeled bulge cells eventually increased in *Sirt7*$^{-/-}$ HFs, indicating that *Sirt7* deletion most likely delays rather blocks HFSC activation. IFE/SG growth and dWAT expansion are highly synchronized with the hair cycle (Li *et al*, 2001; Kruglikov & Scherer, 2016; Reichenbach *et al*, 2018). Consistently, we observed a similar delay in IFE/SG proliferation and dWAT expansion in *Sirt7*$^{-/-}$ mice (Appendix Fig S3C–G).

To assess whether the effects of Sirt7 on HFSCs are cell autonomous, we labeled bulge SCs from *Sirt7*$^{+/+}$, *Sirt7*$^{-/-}$, and *Sirt7*-TG mice as CD34^{+}/integrin-α6^{+} and purified them by FACS from the telogen phase HFs. The cells were allowed to grow for 14 days, as described (Blanpain *et al*, 2004). We found that the *Sirt7* deficiency resulted in a lower number of colonies; by contrast, *Sirt7* overexpression significantly boosted colony formation efficiency (CFE) (Fig 3A and B). The *Sirt7* KO colonies were also smaller in size than the WT colonies; conversely, forced *Sirt7* expression promoted colony expansion (Fig 3C). Of note, we observed a minimal change in the Annexin-V/PI signals between *Sirt7*$^{+/+}$ and *Sirt7*$^{-/-}$ colonies (Appendix Fig S3H). Further, the expression of the stem cell marker Lgr5 (Jaks *et al*, 2008) was equivalent in *Sirt7*$^{+/+}$ and *Sirt7*$^{-/-}$ colonies, arguing against visible differences in stem cell differentiation (Appendix Fig S3I). After four rounds of passaging, *Sirt7*$^{+/+}$, *Sirt7*$^{-/-}$, and *Sirt7*-TG colonies shared comparable CFEs, indicative of equivalent self-renewal abilities. Notably, *Sirt7* KO colonies derived from P4 were still smaller in size (Appendix Fig S3J–L), which is suggestive of deficient proliferation as a result of *Sirt7* loss. Intriguingly, the level of CDK4, which is required for HFSC activation and proliferation (Horsley *et al*, 2008), was significantly downregulated in *Sirt7*$^{-/-}$ but elevated in *Sirt7*-TG colonies (Appendix Fig S3M). Together, these data support that Sirt7 is essential for HFSC activation during HF cycling.

Sirt7 counteracts Nfatc1 activity during HF progression

Multiple pathways are involved in dynamic HFSC activation, including the Wnt/β-catenin, sonic hedgehog (Shh), BMP/SMAD1/5, Notch1, BMP/NFATc1, and TGF-β/SMAD2/3 signaling pathways (Kulessa *et al*, 2000; Andl *et al*, 2002; Oshimori & Fuchs, 2012; Samuelov *et al*, 2012; Wang *et al*, 2016; Bassino *et al*, 2017). To determine which of these signaling pathways might rely on Sirt7, we

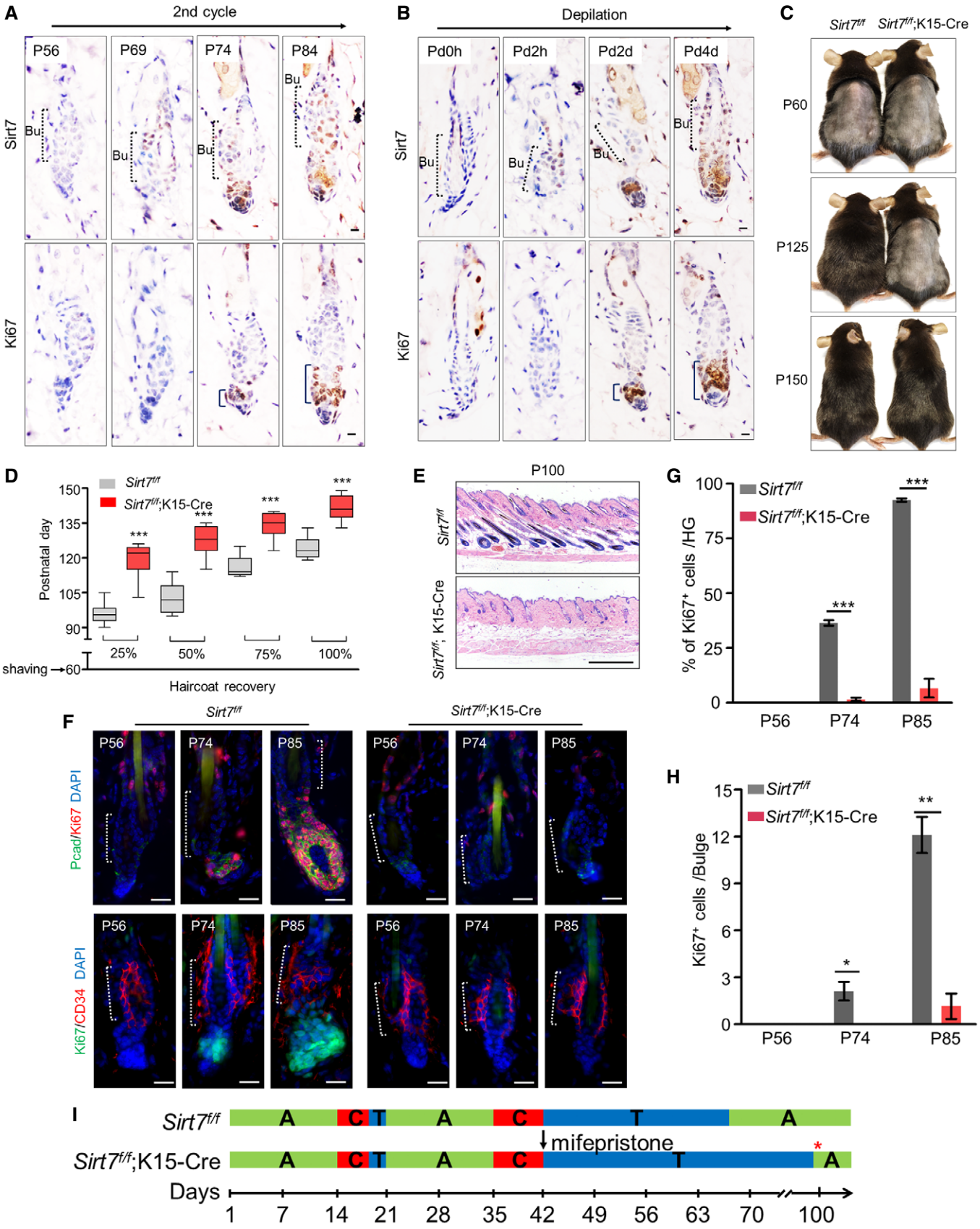
A
2nd cycle
P56
P69
P74
P84
Sirt7
Ki67
Bu
B
Depilation
Pd0h
Pd2h
Pd2d
Pd4d
C
Sirt7f/f
Sirt7f/f;K15-Cre
P60
P125
P150
D
Sirt7f/f
Sirt7f/f;K15-Cre
Postnatal day
shaving
Haircoat recovery
25%
50%
75%
100%
E
P100
Sirt7f/f
Sirt7f/f; K15-Cre
G
% of Ki67+ cells /HG
H
Ki67+ cells /Bulge
F
Pcad/Ki67 DAPI
Ki67/CD34 DAPI
I
Sirt7f/f
Sirt7f/f;K15-Cre
mifepristone
Days

Figure 2.

Figure 2. *Sirt7* deletion delays HFSC activation.

A, B IHC labeling of Sirt7 and Ki67 expression in the skin at different HF phases in the second hair cycle and in the depilation-induced hair cycle in WT mice. P56, P69, P74, and P84 indicate the postnatal day in the second hair cycle. Pd, post-depilation. Dashed line indicates bulge (Bu) of a hair follicle, and solid line indicates the Ki-67-positive staining region.

C The hair coats of *Sirt7*$^{f/f}$ and *Sirt7*$^{f/f}$;K15-Cre mice were clipped at P60, and images were captured on P60, P125, and P150.

D The postnatal day of hair coat recovery by 25, 50, 75, and 100% in shaved *Sirt7*$^{f/f}$ and *Sirt7*$^{f/f}$;K15-Cre mice. n = 6 mice per genotype. Box-and-whisker plots: mid-line, median; box, 25th and 75th percentiles; whiskers, minimum, and maximum.

E H&E staining of the skin in *Sirt7*$^{f/f}$ and *Sirt7*$^{f/f}$;K15-Cre mice at P100.

F Representative immunofluorescence images showing Ki67/Pcad expression (upper) and Cd34/Ki67 expression (lower) in *Sirt7* $^{fl/fl}$ and *Sirt7*$^{f/f}$;K15-Cre HFs on P56, P74, and P85. The white dashed line indicates bulge of hair follicle.

G The percentage of Ki67-positive cells per HG; n = 3 mice and 10 HGs were counted in each mouse.

H Ki67-positive cells per bulge; n = 3 mice and 10 bulges were counted in each mouse.

I Schematic illustrating the HF cycle in *Sirt7*$^{f/f}$ and *Sirt7*$^{f/f}$;K15-Cre mice after mifepristone-induced Cre activation. The arrow indicates the time of mifepristone treatment (details in Materials and Methods); the red star indicates the end of the telogen phase in *Sirt7*$^{f/f}$;K15-Cre HFs.

Data information: Scale bar, 50 μm for IHC and immunofluorescence images, 200 μm for H&E staining images. The data represent the means ± s.e.m. *P < 0.05, **P < 0.01, ***P < 0.001, obtained by Student's t-test.

performed pathway screening by Western blotting. We found that *Sirt7* depletion significantly upregulated but *Sirt7* overexpression attenuated Nfatc1 expression in HFSC colonies, while other genes/pathways were minimally affected (Fig 3D and E, and Appendix Fig S3N). We validated this finding in human keratinocyte HaCaT cells: Here, *SIRT7* knockdown (KD) resulted in significantly elevated NFATc1 expression, whereas *SIRT7* overexpression dose dependently downregulated NFATc1 protein levels (Fig 3F and G).

Nfatc1 is preferentially expressed in HFSCs, regulating dozens of genes to maintain HFSC quiescence (Horsley *et al*, 2008; Keyes *et al*, 2013). The attenuation of Nfatc1 is indispensable for HFSC activation during natural HF cycling, i.e., the telogen-to-anagen transition (Horsley *et al*, 2008). We thus went on to examine whether SIRT7 inhibits NFATc1 transcriptional activity. Using an NFAT-luciferase reporter assay in conjunction with the calcium ionophore ionomycin and phorbol myristate acetate (Ino/PMA), we found that *SIRT7* overexpression in HEK 293T cells significantly inhibited NFATc1 transcriptional activity (Fig 3H). These data indicate a possible causal regulation of Nfatc1 signals by Sirt7.

Intriguingly, the decline in Nfatc1 levels coincided with Sirt7 induction in bulge HFSCs from P56 to P74 in *Sirt7*$^{f/f}$ mice (Fig 3I, left). Conversely, *Sirt7* deletion in HFSCs led to Nfatc1 nuclear retention even at P74 in *Sirt7*$^{f/f}$;K15-Cre mice (Fig 3I, right). We also observed prolonged Nfatc1 nuclear accumulation during the telogen-to-anagen transition in *Sirt7*$^{-/-}$ mice (Appendix Fig S3O) but Nfatc1 elimination even in the early telogen phase in *Sirt7*-TG bulge cells (Fig 3J). These results suggest that Sirt7 counteracts Nfatc1 activity to maintain HFSC quiescence. To test this possibility, we compared the expression profiles of Nfatc1 target genes in HFSC colonies isolated from *Sirt7*$^{-/-}$, *Sirt7*$^{+/+}$, and *Sirt7*-TG mice. Here, Nfatc1 downstream genes were enriched in *Sirt7*$^{-/-}$ HFSCs (Fig 3K). By contrast, a reversal of the gene expression profiles was observed in *Sirt7*-TG HFSCs (Fig 3L). Together, these data implicate that Sirt7 inhibits Nfatc1 signaling in HFs during the telogen-to-anagen transition.

Sirt7 deacetylates Nfatc1

We noticed a marginal change in *NFATc1*/*Nfatc1* mRNA levels upon *Sirt7* KD or KO (Appendix Fig S4A and B), and thus reasoned that Sirt7 might regulate Nfatc1 via a post-translational modification. We first examined whether SIRT7 interacts with NFATc1. Indeed, SIRT7 co-immunoprecipitated with NFATc1 (Fig 4A), and reciprocally, NFATc1 was observed in the anti-SIRT7 immunoprecipitates (Fig 4B). We also detected an endogenous interaction between SIRT7 and NFATc1 in HEK 293T cells (Fig 4C). Furthermore, *in vitro* GST pull-down assay confirmed that the interaction was direct (Fig 4D). We next performed domain mapping to identify which portion of the SIRT7 protein mediates the interaction with NFAT1c. After N- or C-terminal deletion, we found that the SIRT7 catalytic domain (CA) specifically interacted with NFATc1 (Fig 4E). Meanwhile, the NFATc1 regulatory domain (N domain), which regulates NFATc1 stability and nuclear import, bound to SIRT7 (Fig 4F). Moreover, endogenous interaction between SIRT7 and NFATc1 was observed in human keratinocyte HaCaT cells (Fig 4G and H).

SIRT7 belongs to the sirtuin family of deacetylases (Blank & Grummt, 2017). We thus examined whether NFATc1 is deacetylated by SIRT7. Using pan acetyl lysine antibodies, we found that SIRT7 overexpression greatly decreased NFATc1 acetylation levels; this effect was abolished upon nicotinamide (NAM)—a general sirtuin inhibitor—treatment (Fig 4I). By contrast, overexpression of an enzyme dead SIRT7 mutant (H187Y) had little effect on NFATc1 acetylation levels (Fig 4J). Likewise, we observed similar increase in endogenous NFATc1 in HaCaT cells subjected into *SIRT7* knockdown by siRNAs (Appendix Fig S4C). Together, these data implicate that NFATc1 is a target of SIRT7 deacetylase.

We next investigated which deacetylation sites are occupied by SIRT7. We screened for acetyl lysines of NFATc1 after NAM treatment through LC-MS/MS (noting that NAM robustly enhanced overall acetylation levels) and found K612 as a novel NFATc1 acetylation site (Appendix Fig S4D). We reason that K612 is likely a major deacetylation site for sirtuins because the acetylation levels of the NFATc1-K612R mutant were insensitive to NAM (Appendix Fig S4E). These findings encouraged us to examine whether SIRT7 directly deacetylates NFATc1 at K612 *in vitro* and *in vivo*. Here, we found that SIRT7 efficiently erased acetyl groups from WT-NFATc1 but had no marked visible effect on the NFATc1 K612R mutant (Fig 4K and L). SIRTs 1, 2, and 6 have similar functions as SIRT7 in terms of their deacetylase activity (Blank & Grummt, 2017). We thus examined the interactions between NFATc1 and Sirt1/2/6/7. Profoundly, SIRT7 appeared to have the strongest binding of NFATc1 (Appendix Fig S4F), emphasizing the unique role of SIRT7 in NFATc1 regulation.

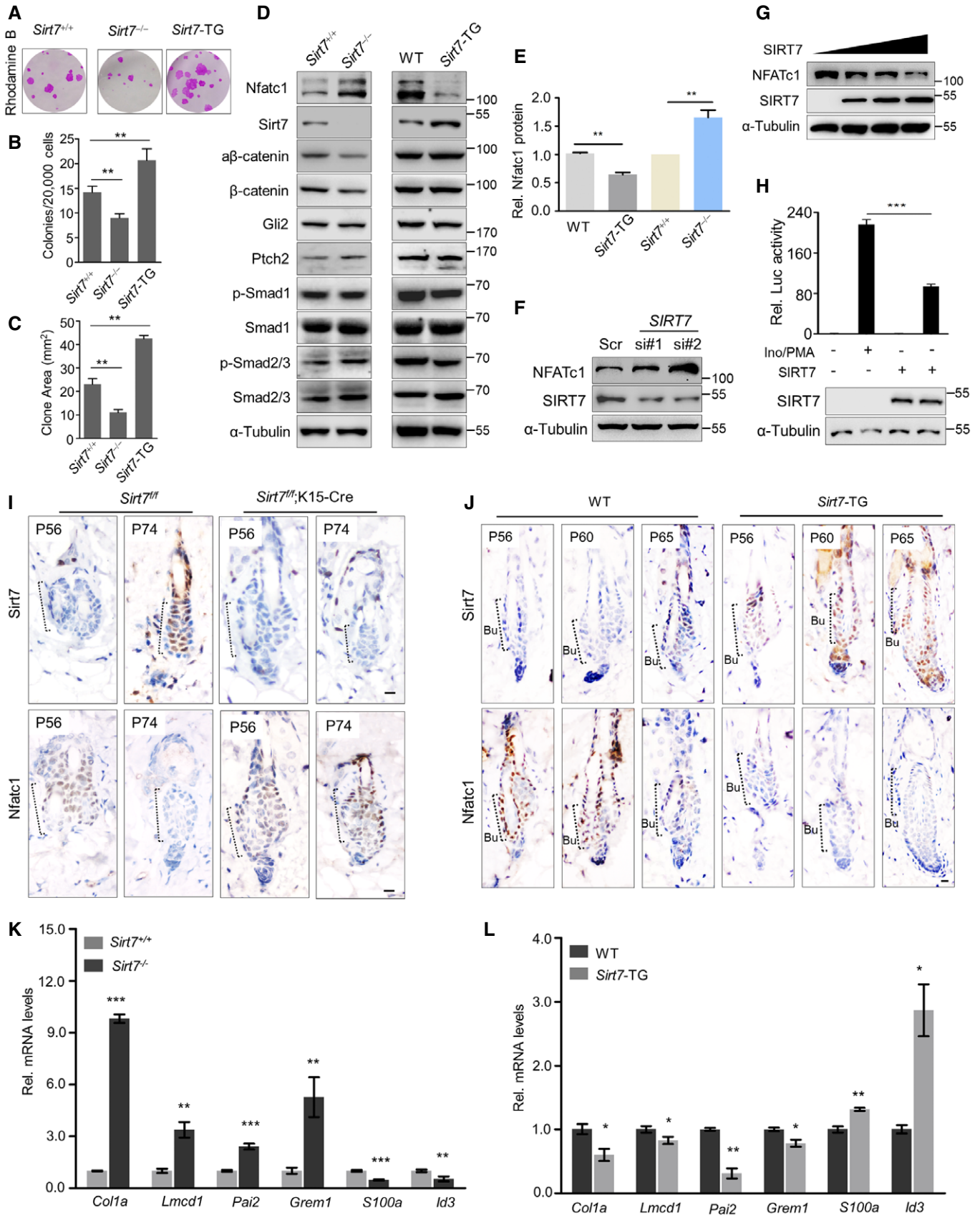
A
Sirt7+/+
Sirt7−/−
Sirt7-TG
Rhodamine B
B
Colonies/20,000 cells
C
Clone Area (mm2)
D
Sirt7+/+
Sirt7−/−
WT
Sirt7-TG
Nfatc1
Sirt7
aβ-catenin
β-catenin
Gli2
Ptch2
p-Smad1
Smad1
p-Smad2/3
Smad2/3
α-Tubulin
E
Rel. Nfatc1 protein
F
SIRT7
Scr
si#1
si#2
NFATc1
SIRT7
α-Tubulin
G
SIRT7
NFATc1
SIRT7
α-Tubulin
H
Rel. Luc activity
Ino/PMA
SIRT7
SIRT7
α-Tubulin
I
Sirt7f/f
Sirt7f/f;K15-Cre
P56
P74
Sirt7
Nfatc1
J
WT
Sirt7-TG
P56
P60
P65
Sirt7
Nfatc1
Bu
K
Sirt7+/+
Sirt7-/-
Rel. mRNA levels
Col1a
Lmcd1
Pai2
Grem1
S100a
Id3
L
WT
Sirt7-TG
Rel. mRNA levels
Col1a
Lmcd1
Pai2
Grem1
S100a
Id3

Figure 3.

Figure 3. Altered expression of Nfatc1 in *Sirt7*-modified mice.

A Representative colonies formed by *Sirt7*$^{+/+}$, *Sirt7*$^{-/-}$, and *Sirt7*-TG bulge SCs that were purified from telogen-phase HFs and allowed to grow for 2 weeks.

B, C Quantifications of colony number and size in (A); $n = 3$ mice per genotype.

D, E Immunoblot analysis of the indicated proteins in HFSC colonies from *Sirt7*$^{+/+}$, *Sirt7*$^{-/-}$, and *Sirt7*-TG mice (D) and Nfatc1 protein levels were quantified using ImageJ Plus 6.0 (E, $n = 3$ mice for each group).

F Immunoblot analysis of the NFATc1 expression level in human keratinocyte HaCaT cells treated with *SIRT7* siRNAs.

G Immunoblot analysis of the NFATc1 expression in the presence of ectopic SIRT7 expression in HaCaT cells.

H NFATc1 luciferase activity was monitored in HEK293T cells after the indicated treatments ($n = 3$). The relative luciferase activity was determined by dual-luciferase reporter assay.

I, J IHC analyses of Nfatc1 expression in hair follicles of *Sirt7*$^{f/f}$, *Sirt7*$^{f/f}$;K15-Cre, and *Sirt7*-TG mice at the indicated time points. The black dashed line indicates the bulge (Bu) of hair follicle.

K, L qPCR analysis of Nfatc1-targeted genes in HFSC colonies cultured from *Sirt7*$^{+/+}$, *Sirt7*$^{-/-}$, and *Sirt7*-TG mice, $n = 3$ for each genotypes.

Data information: Scale bar, 50 μm for the IHC images. The data represent the means ± s.e.m. $^{*}P < 0.05$, $^{**}P < 0.01$, $^{***}P < 0.001$, determined by Student's *t*-test.

Source data are available online for this figure.

SIRT7 promotes nuclear NFATc1 degradation

NFATc1 is prone to phosphorylation and subsequent degradation in the cytoplasm (Porter *et al*, 2000). We thus asked whether there is an intrinsic interplay between NFATc1 deacetylation and phosphorylation. We found that a constitutively active form of GSK-3β (CA-GSK-3β), which phosphorylates nuclear NFATc1 at the SP motif (Beals *et al*, 1997b; Neal & Clipstone, 2001), significantly attenuated NFATc1 acetylation levels. By contrast, LiCl, a GSK-3β inhibitor, inhibited this phosphorylation but increased NFATc1 acetylation (Fig 4M). Notably, CA-NFATc1, which mimics constitutive de-phosphorylation by mutating serines to alanines in SRR/SP (Neal & Clipstone, 2003), exhibited hyper-acetylation (Fig 4N).

We then asked whether SIRT7 regulates NFATc1 phosphorylation via K612 deacetylation. As shown, the K612R mutant, mimicking hypoacetylation, possessed much higher phosphorylation levels than WT and K612Q, which mimics the hyper-acetylated form of NFATc1 (Fig 4O). Given that NFATc1 phosphorylation is causally linked to degradation, we next explored whether SIRT7-mediated deacetylation contributes to NFATc1 degradation. To this end, we constructed a HEK293T cell line with stable expression of ectopic *NFATc1* to exclude the potential effects of transcription. A cycloheximide (CHX) chase assay showed that ectopic *SIRT7* expression accelerated NFATc1 degradation compared to an empty vector (EV) control (Fig 5A and B). Conversely, endogenous Nfatc1 protein was more stable in *Sirt7*$^{-/-}$ mouse keratinocyte (MK) cells and *SIRT7* knockdown HaCaT cells (Fig 5C and D, and Appendix Fig S4G). In addition, HA-SIRT7 promoted the NFATc1 protein turnover rate, while the H187Y mutant had negligible effects (Fig 5E and F).

As SIRT7 mainly localizes in the nucleus, we asked whether SIRT7 deacetylase activity mediates NFATc1 degradation in the nucleus. Indeed, CA-NFATc1, which confers constitutive nuclear import, was more sensitive to degradation upon SIRT7 overexpression in HEK293T cells (Fig 5G and H). Of note, MG132 treatment inhibited NFATc1 degradation induced by ectopic SIRT7, indicating that this event occurs in a proteasome-dependent manner. In addition, compared to WT NFATc1, the K612R mutant underwent faster turnover, underlining that SIRT7-mediated deacetylation directly affects NFATc1 degradation (Fig 5I and J).

We next examined how SIRT7 mediates NFATc1 degradation. We first assessed the activity of the ubiquitination–proteasome system. Surprisingly, *SIRT7* overexpression had little effect on NFATc1 ubiquitination (Appendix Fig S4H), suggesting that ubiquitination-independent proteasomal degradation occurs. PA28γ is a proteasome activator that predominantly localizes in the nucleus (Wilk *et al*, 2000). Of particular note, hair regrowth in *Pa28γ*$^{-/-}$ mice is delayed to a similar degree as that seen in *Sirt7*$^{-/-}$ mice (Li *et al*, 2013). We thus asked whether SIRT7 regulates NFATc1 degradation via PA28γ. Indeed, FLAG-tagged PA28γ interacted with NFATc1, and this interaction was enhanced upon *SIRT7* overexpression (Fig 5K). Consistently, *SIRT7* knockdown prevented the binding of endogenous NFATc1 and PA28γ (Fig 5L), while *SIRT7* overexpression caused the opposite effect in HaCaT cells (Appendix Fig S4I). Further, through truncated domain analysis, we found that PA28γ recognized the C-terminal DNA binding domain of NFATc1, in which K612 resides (Appendix Fig S4J). *PA28γ* knockdown attenuated SIRT7-mediated NFATc1 degradation (Fig 5M and N, and Appendix Fig S4K), while overexpression of HA-SIRT7, but not the H187Y mutant, promoted NFATc1 binding to PA28γ (Fig 5O). We thus conclude that SIRT7 promotes nuclear NFATc1 degradation via PA28γ and a deacetylation-mediated interaction.

Cyclosporin A treatment restores hair growth in *Sirt7*$^{-/-}$ mice

Having identified a mechanism by which Sirt7 regulates Nfatc1 stability, we next tested whether Nfatc1 underlies Sirt7-mediated HF cycling progression. As NFATc1 suppresses HFSC proliferation, we examined whether SIRT7 mediated deacetylation of NFATc1 imposes growth inhibition in actively proliferative HaCaT cells. As determined by 2-D single cell colony-forming assay, cells expressing NFATc1-K612Q generated fewer tight colonies and displayed significant expansion arrest compared to cells expressing NFATc1-K612R (Appendix Fig S5A and B).

The Ca^{2+}/calmodulin-dependent serine phosphatase calcineurin dephosphorylates NFATc1 to promote its nuclear import (Goldstein *et al*, 2014). Cyclosporin A (CsA), a potent calcineurin inhibitor, suppresses this import and thus blocks NFATc1 nuclear activity (Hogan *et al*, 2003). After shaving the back hair at telogen phase, we exposed the skin of *Sirt7*$^{-/-}$ mice to CsA, aiming to inhibit Nfatc1. IHC analysis showed that CsA treatment significantly attenuated Nfatc1 nuclear accumulation at P84 in *Sirt7*$^{-/-}$ mice, while the vehicle-treated *Sirt7*$^{-/-}$ HFs maintained a normal nuclear level of Nfatc1 (Fig 6A and B). *Sirt7*$^{-/-}$ HFs exposed to CsA showed strong Ki-67 staining at P84 at a similar level as *Sirt7*$^{+/+}$ HFs, indicating

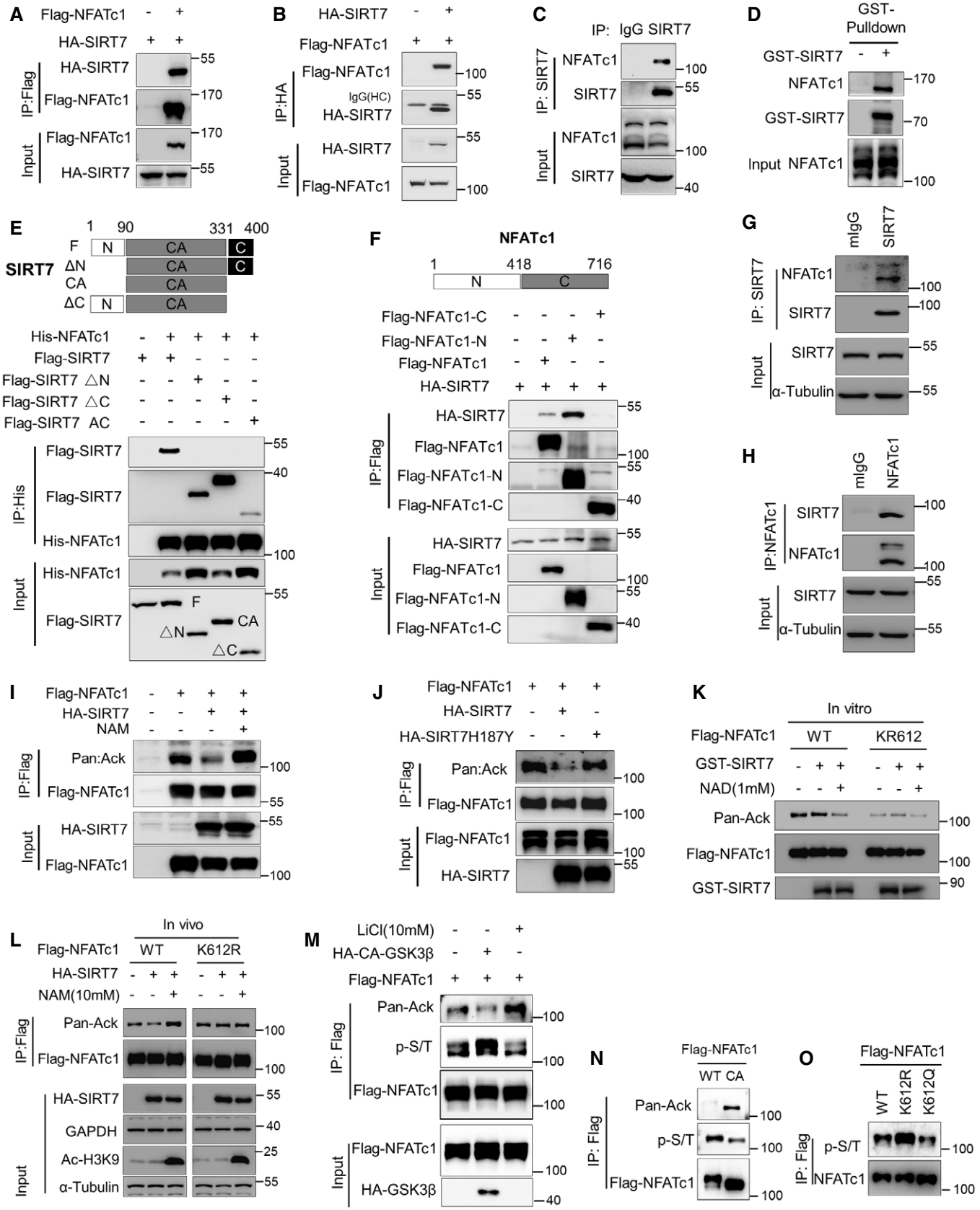
A
Flag-NFATc1 - +
HA-SIRT7 + +
IP:Flag
HA-SIRT7
Flag-NFATc1
Input
Flag-NFATc1
HA-SIRT7
55
170
170
55
B
HA-SIRT7 - +
Flag-NFATc1 + +
IP:HA
Flag-NFATc1
IgG(HC)
HA-SIRT7
Input
HA-SIRT7
Flag-NFATc1
100
55
55
100
C
IP: IgG SIRT7
IP: SIRT7
NFATc1
SIRT7
Input
NFATc1
SIRT7
100
55
100
40
D
GST-Pulldown
GST-SIRT7 - +
NFATc1
GST-SIRT7
Input NFATc1
170
70
100
E
1 90 331 400
F N CA C
SIRT7 ΔN CA C
CA CA
ΔC N CA
His-NFATc1 - + + + +
Flag-SIRT7 + + - - -
Flag-SIRT7 △N - - + - -
Flag-SIRT7 △C - - - + -
Flag-SIRT7 AC - - - - +
IP:His
Flag-SIRT7
Flag-SIRT7
His-NFATc1
Input
His-NFATc1
Flag-SIRT7
F
CA
△N
△C
55
40
100
55
F
NFATc1
1 418 716
N C
Flag-NFATc1-C - - - +
Flag-NFATc1-N - - + -
Flag-NFATc1 - + - -
HA-SIRT7 + + + +
IP:Flag
HA-SIRT7
Flag-NFATc1
Flag-NFATc1-N
Flag-NFATc1-C
Input
HA-SIRT7
Flag-NFATc1
Flag-NFATc1-N
Flag-NFATc1-C
55
100
55
40
55
100
55
40
G
mIgG SIRT7
IP: SIRT7
NFATc1
SIRT7
Input
SIRT7
α-Tubulin
100
100
55
55
H
mIgG NFATc1
IP:NFATc1
SIRT7
NFATc1
Input
SIRT7
α-Tubulin
100
100
55
55
I
Flag-NFATc1 - + + +
HA-SIRT7 - - + +
NAM - - - +
IP:Flag
Pan:Ack
Flag-NFATc1
Input
HA-SIRT7
Flag-NFATc1
100
55
55
100
J
Flag-NFATc1 + + +
HA-SIRT7 - + -
HA-SIRT7H187Y - - +
IP:Flag
Pan:Ack
Flag-NFATc1
Input
Flag-NFATc1
HA-SIRT7
100
100
100
55
K
In vitro
Flag-NFATc1 WT KR612
GST-SIRT7 - + + - + +
NAD(1mM) - - + - - +
Pan-Ack
Flag-NFATc1
GST-SIRT7
100
100
90
L
In vivo
Flag-NFATc1 WT K612R
HA-SIRT7 - + + - + +
NAM(10mM) - - + - - +
IP:Flag
Pan-Ack
Flag-NFATc1
Input
HA-SIRT7
GAPDH
Ac-H3K9
α-Tubulin
100
100
55
40
25
55
M
LiCl(10mM) - - +
HA-CA-GSK3β - + -
Flag-NFATc1 + + +
IP: Flag
Pan-Ack
p-S/T
Flag-NFATc1
Input
Flag-NFATc1
HA-GSK3β
100
100
100
100
40
N
Flag-NFATc1
WT CA
IP: Flag
Pan-Ack
p-S/T
Flag-NFATc1
100
100
100
O
Flag-NFATc1
WT K612R K612Q
IP: Flag
p-S/T
NFATc1
100
100

Figure 4.

Figure 4. SIRT7 deacetylates NFATc1 at K612.

A, B Immunoblot analysis of the interactions between ectopic HA-SIRT7 and FLAG-NFATc1in HEK293T cells.
C Co-immunoprecipitation (CoIP) between endogenous NFATc1 and SIRT7 in HEK293T cells.
D Immunoblots showing endogenous NFATc1 pull down by GST-SIRT7 in HEK293T cells.
E Immunoblot analysis of HA-SIRT7 WT and various mutants in the anti-His-NFATc1 immunoprecipitates. ΔN indicates N-terminal deletion; ΔC indicates C-terminal deletion; AC indicates N-terminal and C-terminal deletion.
F Immunoblot analysis of HA-SIRT7 levels in truncated FLAG-NFATc1 immunoprecipitates. N indicates the N-terminal domain; C indicates C-terminal domain.
G, H Immunoblot analysis of the interactions between endogenous NFATc1 and SIRT7 in keratinocyte HaCaT cells.
I, J Immunoblot analysis of NFATc1 acetylation levels in response to the indicated treatments.
K, L Immunoblot analysis of NFATc1-WT/K612R acetylation based on SIRT7 deacetylation assays *in vitro* (K) and *in vivo* (L).
M, N Immunoblots showing NFATc1 pan phosphorylation (probing to anti-S/T antibody) and acetylation levels under the indicated treatments.
O Immunoblot analysis of NFATc1 phosphorylation among K612 mutants, noting that K612R represents deacetylation while K612Q hyper-acetylation.

Source data are available online for this figure.

HFSC activation and anagen entry (Fig 6C and D). Furthermore, most of the CsA-treated *Sirt7*$^{-/-}$ HFs progressed to anagen phase, whereas adjacent untreated skin HFs remained quiescent (Fig 6E). Consequently, it seems that CsA treatment largely improved hair coat recovery in *Sirt7*$^{-/-}$ mice (Fig 6F). Altogether, these data suggest that Nfatc1 accumulation in telogen phase contributes to the HF cycling delay in *Sirt7*$^{-/-}$ mice.

Sirt7 overexpression prevents age-related hair dysfunction

Aging-related hair thinning and hair loss are prominent characteristics in humans and mice. These phenotypes are largely attributable to the extended dormancy of HFSCs. As Sirt7 is associated with aging progression and it initiates HFs cycling, we postulated whether it might also be involved in age-related hair dysfunction. Interestingly, we observed a significantly lower level of *Sirt7* in aged HFs (18 months), regardless of telogen or anagen phase, compared to young HFs (3 months) (Appendix Fig S5C). We confirmed this downregulation in Sirt7 expression in HFSCs from aged mice (Fig 7A). Consistently, stronger nuclear Nfatc1 retention coincided with Sirt7 downregulation in aged HFSCs compared to young HSFCs at telogen phase (Fig 7B–D). Of note, γH2AX foci were significantly prominent in the 18 months old mice, indicating the aging HFs (Appendix Fig S5D and E).

We next asked whether *Sirt7* decline accelerates aging-related hair thinning and loss. *Sirt7*$^{-/-}$ mice displayed severely diffuse patterns of hair thinning and expressed higher Nfatc1 levels in HFSCs compared to *Sirt7*$^{+/+}$ mice at 15 months of age (Fig 7E–G). We then examined whether reinforcing *Sirt7* expression could restore hair growth in aged mice. In our depilation model, we observed faster hair regrowth in plucked *Sirt7*-TG mice than in control mice at 20 months of age (Fig 7H and I). Moreover, aged *Sirt7*-TG mice showed a faster hair coat recovery rate compared to WT mice (Fig 7J). Importantly, *Sirt7*-TG mice exhibited a higher density of hair shafts, even at 28 months of age compared to WT mice (Fig 7K). These data suggest that the Sirt7–Nfatc1 axis regulates age-related hair dysfunction and that boosting Sirt7 might benefit hair regeneration.

Discussion

Adult stem cells are essential to help drive tissue regeneration and maintain homeostasis in multiple organs over a lifetime of environmental and physical insult to the body. Depletion or permanent quiescence of the stem cell pool underlies degeneration in various organs during aging (Ermolaeva *et al*, 2018). The sirtuin family members Sirt1, Sirt6, and Sirt7 are critical to ensuring hematopoietic stem cell homeostasis and function (O'Callaghan & Vassilopoulos, 2017). Here, we identified SIRT7 as a key activator of the telogen-to-anagen transition in cycling HFs: It achieves this function by promoting deacetylation-induced degradation of NFATc1.

Sirt7 levels sharply decrease in HFSCs with aging; this decrease contributes, at least in part, to the prolonged HFSC quiescence observed in aged mice. When we reinforced *Sirt7* in old mice by overexpression, we observed a significant improvement in aging-associated hair dysfunction. Sirt1 and Sirt6 possess stronger deacetylase activity than Sirt7 (Wu *et al*, 2018): This finding elicits the interesting question of whether Sirt1, Sirt6, and Sirt7 have redundant roles in HFSCs. Unlike Sirt7, we did not observe any obvious or strong interaction between Sirt1, Sirt2, Sirt6, and Nfatc1 (Appendix Fig S4F), suggesting that these sirtuin family members are unlikely to act as Nfatc1 deacetylases in this context. Moreover, neither *Sirt7* knockout nor overexpression markedly affected *Sirt1*, *Sirt2*, or *Sirt6* mRNA levels in HFSC colonies (Appendix Fig S5F and G), arguing against the existence of potential functional redundancy. These data suggest that Sirt7 might have a rather specific role in regulating HF cycling.

In the telogen phase, BMP signaling transcriptionally upregulates NFATc1 and activates the calcium–NFATc1–CDK4 circuitry to govern HFSC quiescence (Horsley *et al*, 2008; Fujimura *et al*, 2011; Keyes *et al*, 2013). When calcium signaling is activated, NFATc1 is dephosphorylated by calcineurin, exposing the masked nuclear localization signals (NLSs), and then translocates to the nucleus to regulate transcription (Flanagan *et al*, 1991; Clipstone & Crabtree, 1992; Gafter-Gvili *et al*, 2003). Calcineurin dephosphorylates the serine-rich region (SRR) and the serine-proline rich 1 (SP1), SP2 and SP3 motifs within the NFATc1 amino terminus (Beals *et al*, 1997a). Several studies disclose that PCAF/P300 acetylases are associated with NFATc1 nuclear import (Garcia-Rodriguez & Rao, 1998). NFATc1 acetylation strengthens its stabilization and nuclear retention and consequently sustains NFATc1-induced signaling that regulates diverse physiological functions (Kim *et al*, 2011). To initiate anagen entry, activating signals antagonize BMP signaling to terminate *NFATc1* transcription (Horsley *et al*, 2008); however, nuclear-retained NFATc1 might still serve to resist or delay anagen entry.

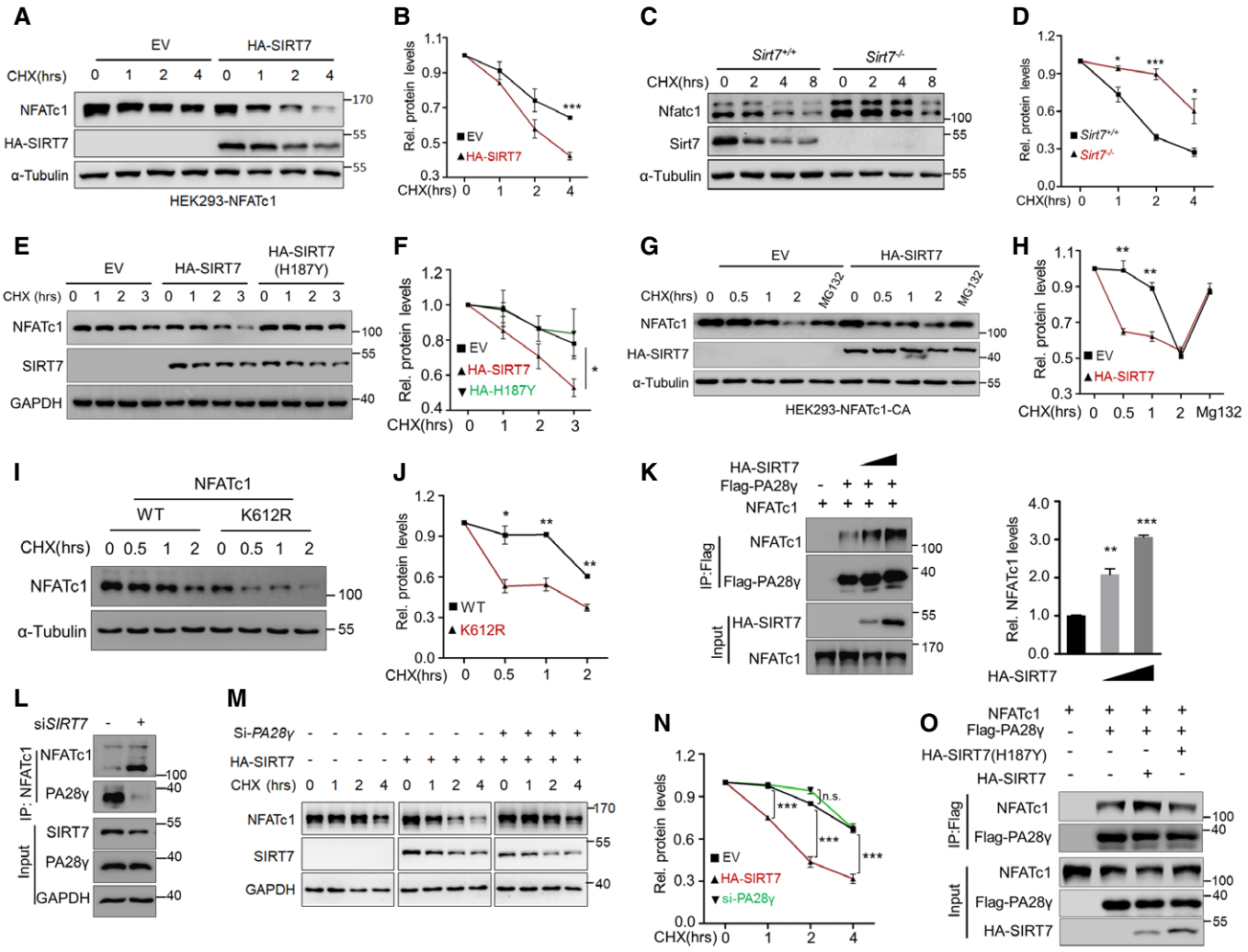

Figure 5. SIRT7 promotes NFATc1 degradation via PA28γ.

A Representative immunoblots showing NFATc1 degradation in HEK293T cells stably overexpressing NFATc1 in the presence of cycloheximide (CHX), with or without SIRT7 overexpression.

B Quantification of NFATc1 levels in (A) from 3 independent experiments.

C Immunoblots of Nfatc1 protein levels in *Sirt7*$^{+/+}$ and *Sirt7*$^{-/-}$ keratinocytes.

D Quantification of Nfatc1 levels in (C) from 3 independent experiments.

E, F Immunoblots (E) and related quantitative data (F, n = 3) showing NFATc1 protein levels in HEK293T cells overexpressing wild-type HA-SIRT7 or a SIRT7 enzyme-dead mutant (H187Y).

G, H Immunoblots (G) and quantitative data (H, n = 3) showing NFATc1 levels in HEK293T cells transfected with NFATc1-CA, with or without ectopic SIRT7, treated with MG132.

I, J Immunoblots (I) and related quantitative data (J, n = 3) showing NFATc1-WT and NFATc1-K612R protein turnover in HEK293T cells.

K, L Immunoblots showing the interaction (by co-immunoprecipitation) between ectopic NFATc1/PA28γ in HEK293T cells (K) or endogenous NFATc1/PA28γ in HaCaT cells (L) after manipulating SIRT7 levels.

M, N Immunoblot (M) and quantitative data (N, n = 3) analysis of NFATc1 levels upon overexpression of HA-SIRT7 with or without *PA28γ* oligo siRNA treatment.

O Co-immunoprecipitation between NFATc1 and PA28γ in HEK293T cells cotransfected with WT HA-SIRT7 or an enzyme-dead mutant (H187Y).

Data information: The data represent the means ± s.e.m. *P < 0.05, **P < 0.01, ***P < 0.001, determined by Student's t-test.

Source data are available online for this figure.

GSK-3β-mediated phosphorylation of nuclear NFATc1 promotes NFATc1 nuclear export (Beals *et al*, 1997b; Neal & Clipstone, 2001); here, NFATc1 undergoes ubiquitination and proteasomal degradation in the cytoplasm in resting cells (Porter *et al*, 2000; Crabtree & Olson, 2002). We found that Sirt7-mediated K612 deacetylation and GSK-3β-mediated phosphorylation synergize to regulate nuclear NFATc1. PA28γ located in the nucleus activates 20S proteasome-mediated proteolysis (Realini *et al*, 1997; Mao *et al*, 2008). Although the precise mechanism as to how PA28γ recognizes its substrates is unclear, we know that it elicits efficient proteolysis

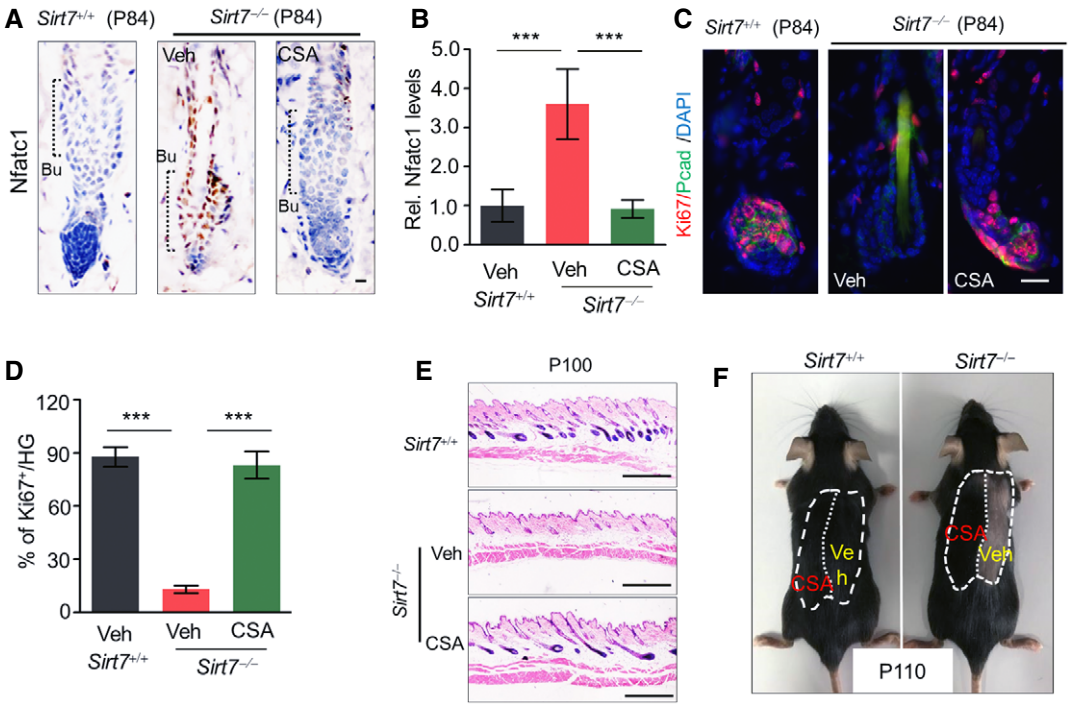

Figure 6. Cyclosporin A abrogates HF cycling delay induced by *Sirt7* deletion.

A IHC staining of Nfatc1 expression in HFs on P84 in $Sirt7^{+/+}$ and $Sirt7^{-/-}$ mice with or without Cyclosporin A (CsA) treatment. The black dashed line indicates bulge (Bu) of hair follicle.

B Quantitative analysis of Nfatc1 levels in (A, n = 10 hair follicles) using ImageJ plus 6.0.

C Immunofluorescent staining of Ki67 and Pcad at P84 in $Sirt7^{+/+}$ and $Sirt7^{-/-}$ HFs with or without CsA treatment.

D The percentage of Ki67-positive cells per HG in (C, n = 10 hair follicles).

E H&E staining of the skin in the indicated treatment groups at P100.

F Representative images showing hair coat recovery after the indicated treatments. The dashed circle indicates the shaved area; the dotted line indicates the hair growth boundary.

Data information: Scale bars, 50 μm for the IHC and immunofluorescence images and 200 μm for the H&E images. The data represent the means ± s.e.m. ***$P < 0.001$, determined by Student's t-test.

after basic residues (Wilk *et al*, 2000; Li *et al*, 2001). Interestingly, PA28γ strongly interacts with the NFATc1 DNA binding domain (DBD), wherein K612 is embedded. The K612R mutation, which mimics hypoacetylated NFATc1, enhances the interaction with PA28γ and subsequent degradation. We speculate that K612 deacetylation by SIRT7 releases a free basic lysine that helps to fully expose the basic residue cluster (GKKM) in NFATc1 and activate PA28γ-mediated proteasome hydrolysis. We propose that Sirt7-mediated Nfatc1 deacetylation and subsequent degradation might act as a key mechanism to quickly eliminate nuclear Nfatc1, thus granting quick telogen-to-anagen transition. Indeed, quiescent stem cells minimize the transcription and translation rate to reserve the limited energy supply for normal function maintenance (Ermolaeva *et al*, 2018).

Despite these findings, it remains unanswered how *Sirt7* expression is manipulated during the telogen-to-anagen transition. TGF-β signaling is transiently activated in HFSCs at an early stage of the hair cycle (Oshimori & Fuchs, 2012). Data from several studies have suggested that SIRT7 is associated with TGF-β signaling (Araki *et al*, 2015; Tang *et al*, 2017, 2020). In this regard, future work should study whether TGF-β signaling regulates *Sirt7* expression during HF phase transition. How severe loss of *Sirt7* expression in HFSCs occurs in aged mice is also an interesting question to address in future studies. HFSCs are long-lived proliferative cells that suffer from damage accumulation and epigenetic alterations during repetitive HF cyclings, thus leading to aging-related permanent quiescence (Matsumura *et al*, 2016). Consistently, prominent γH2AX is observed in HFs from aged mice (Appendix Fig S5D and E). Of note, SIRT7 is important for genome maintenance (Li *et al*, 2016; Vazquez *et al*, 2016; Tang *et al*, 2019); therefore, in aged mice, a decline in *Sirt7* will not only fail to evoke HFSCs from quiescence, but might also cause DNA damage accumulation in HFSCs leading to permanent exit from the cell cycle. Addressing the mechanism that regulates dynamic *Sirt7* expression during HF cycling might, therefore, provide a promising target for clinical translation.

In summary, we show that Sirt7 facilitates the onset of the hair cycle by promoting NFATc1 degradation in a deacetylation-dependent manner. An aging-conferred decline in *Sirt7* levels reinforces HFSC quiescence, while Sirt7-restoration ameliorates aging-related hair dysfunction. These findings highlight SIRT7 as a potential new target for ameliorating aging-related hair loss.

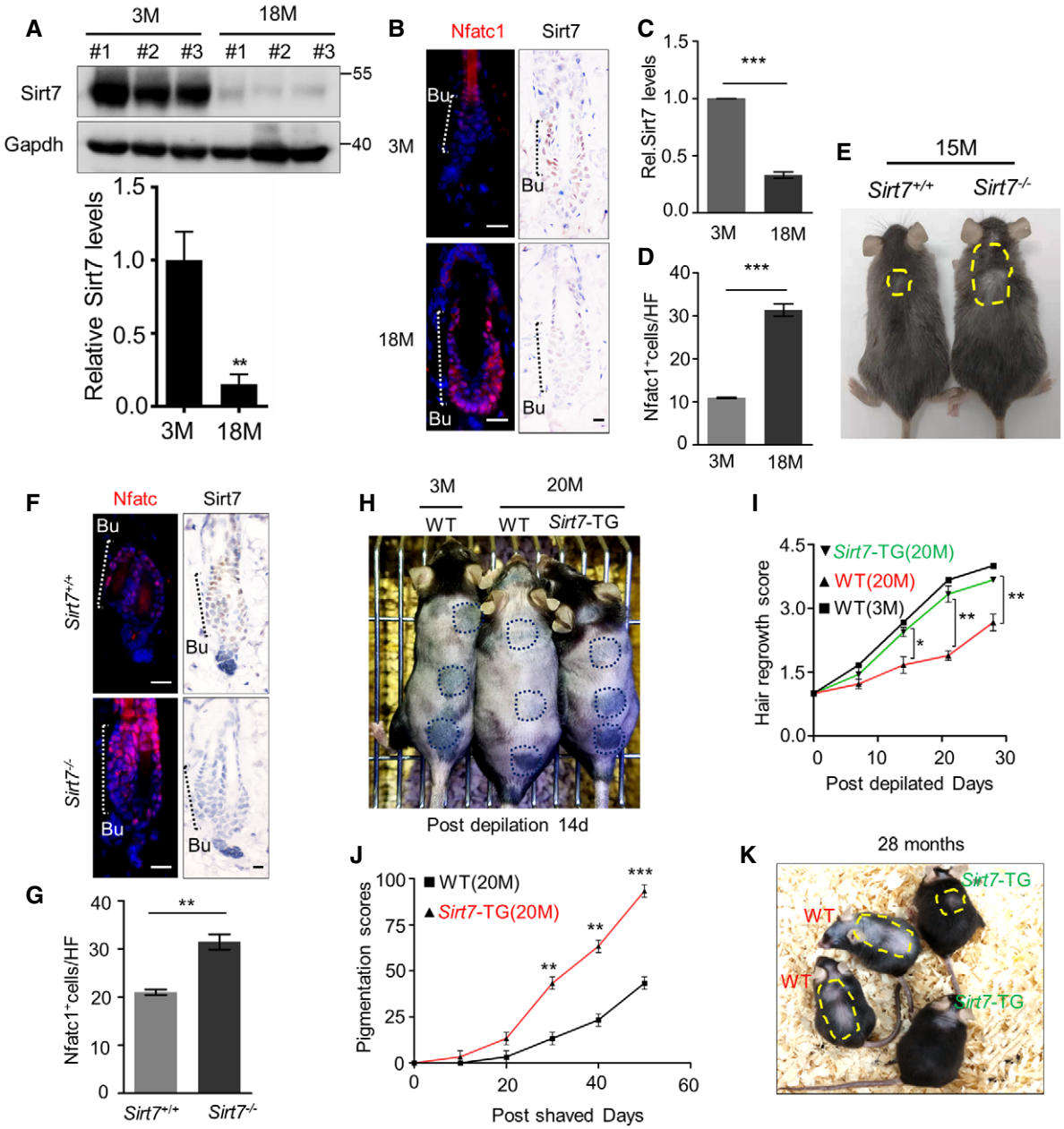

Figure 7. Sirt7 associates with aging-related hair dysfunction.

A Immunoblot analysis of Sirt7 expression in young (3M) and aged (18M) HFSCs. #1, #2, #3 represented individual mice. Below, quantification of Sirt7 protein levels; n = 3 mice for each group; the Y-axis represents the relative band intensity (measured with ImageJ®) normalized to the signal in young mice.

B–D Immunofluorescence and IHC staining of Nfatc1 and Sirt7 in HFs of young (3 months) and old (18 months) mice (B), and the relative levels of Sirt7 and Nfatc1-positive cells in the bulge (C, D). The white/black dashed line indicates bulge (Bu) of hair follicle.

E Images were captured of the hair coats of *Sirt7*$^{+/+}$ and *Sirt7*$^{-/-}$ mice at 15 months. The yellow dashed lines indicate hair thinning or hair loss.

F Immunofluorescence and IHC staining of Nfatc1 and Sirt7 in HFs of 15-month-old *Sirt7*$^{+/+}$ and *Sirt7*$^{-/-}$ mice. The white/black dashed line indicates bulge (Bu) of hair follicle.

G Quantification of Nfatc1-positive cells per bulge in (F, n = 10 hair follicles).

H Images captured of the skin in the plucked regions (blue dotted lines) of WT (3 months), aged WT (20 months) and aged *Sirt7*-TG mice (20 months), 14 days after depilation. Pigmentation of the skin indicates hair regrowth. n = 3 mice per genotype.

I Hair regrowth scores were analyzed for young WT, old WT and old *Sirt7*-TG mice in (H), n = 3 mice for each group.

J The hair coat recovery score (described in Materials and Methods) after the back hair of old WT and old *Sirt7*-TG mice was shaved. n = 3 mice per genotype.

K Images captured of the hair coats of WT and *Sirt7*-TG mice at 28 months of age. The yellow dashed lines indicate the hair thinning or hair loss regions.

Data information: Scale bars, 50 μm for the IHC and immunofluorescence images. The data represent the means ± s.e.m. *P < 0.05, **P < 0.01, ***P < 0.001, determined by Student's t-test.

Source data are available online for this figure.

Materials and Methods

Animals

Sirt7$^{-/-}$ mice were generated by Cyagen by CRISPR-Cas9 technique (Guangzhou, China). The *Sirt7*$^{-/-}$ mice were backcrossed for at least three generations to separate potential off-target deletions. *Sirt7*-TG mice were generated and bred as previously described (Tang *et al*, 2017). *Sirt7* overexpression was induced by oral application of Dox diluted in the drinking water to a final concentration of 1 mg/ml at the indicated time for at least 7 days. For *in vivo* experiments using CsA, mice dorsal skins were treated with 0.5% CsA or vehicle (64% EtOH, 20% propyleneglycol, 16% water) for 7 days. A K15-CrePGR mouse was used to achieve *Sirt7* deletion in HFSCs. To activate Cre expression, mice were treated with mifepristone topically on their dorsal skin during telogen once a day for 7 days (12 mg in ethanol), as previously described (Morris *et al*, 2004; Lay *et al*, 2018). All mice were maintained under specific-pathogen-free conditions and the procedures were performed in accordance with the instructions and permissions of the ethical committee on the Use of Live Animals in Teaching and Research of Shenzhen University.

Hair cycle analysis

Hair cycle analyses were based on skin pigmentation, as previously described (Stenn & Paus, 2001). In brief, shaved hair coat recovery values from 0 to 100% were calculated based on skin pigmentation levels and hair shaft density (Chai *et al*, 2019). For example, 0% indicated no hair growth (and no pigmentation); 50% indicated full-length hair growth on 50% of the dorsal skin area or pigmentation on 100% of the dorsal skin area without hair shafts; 70% indicated full-length hair growth on 70% of the dorsal skin or pigmentation on 100% of dorsal skin with 30–40% hair shafts; 100% indicated full-length hair growth on 100% of the dorsal skin.

Immunohistochemical (IHC) and immunofluorescence (IF) staining

Back skins were harvested from mid-dorsal areas based on hair cycle stages that were determined as described above (Muller-Rover *et al*, 2001; Chai *et al*, 2019). H&E staining and IHC/IF were performed as previously described (Oshimori & Fuchs, 2012). The antibodies used for IHC or IF included the following: SIRT7 (EMD Millipore, ABE103, 1:50 dilution), Ki67 (Abcam, ab15580, 1:600 dilution), P-cadherin (R&D System, AF761, 1:200 dilution), CD34 (eBioscience, 14-0341-82, 1:400 dilution), NFATc1 (Santa Cruz, sc-7294, 1:50 dilution), anti-Brdu (Abcam, ab6326, 1:200 dilution), SIRT1 (Abcam, ab110304, 1:100 dilution), and SIRT6 (Abcam, ab62739, 1:100 dilution). The following fluorescence-labeled secondary antibodies were used in current study: Donkey anti-Mouse IgG(H+L), Alexa Fluor Plus 594 (Invitrogen, A32744, 1:500 dilution); Donkey anti-Rabbit IgG(H+L), Alexa Fluor Plus 594 (Invitrogen, A32754, 1:500 dilution); Donkey anti-Rabbit IgG(H+L), Alexa Fluor Plus 488 (Invitrogen, A32790, 1:500 dilution), Donkey anti-Rat IgG(H+L), Alexa Fluor Plus 594 (Invitrogen, A-21209, 1:500 dilution); and Donkey anti-goat IgG(H+L), Alexa Fluor Plus 488 (Invitrogen, A-11055, 1:500 dilution).

Cell culture

HEK293T (embryonic kidney cell line) and HaCaT (immortalized human keratinocyte cell line) cells were cultured in Dulbecco's modified Eagle's medium (DMEM, high glucose) with 10% FBS and penicillin–streptomycin antibiotics in a 5% CO_2 incubator at 37°C. All cells were tested by PCR to confirm that they were not contaminated by mycoplasma (TaKaRa PCR Mycoplasma Detection Set, Japan). To isolate HFSCs, HF cells were isolated by fluorescence-activated cell sorting (FACS) labeling stem cell surface marker α6-integrin (CD49f) and CD34. For HFSC functional analyses, equal numbers of live cells (20,000) were plated (n = 3) onto mitomycin C (MMC)-treated dermal fibroblasts in E-media supplemented with 15% serum and 0.3 mM calcium. After growing for 14 days, the cells were fixed and stained with 1% (wt/vol) rhodamine B (MCE). Colony numbers were counted, and the colony size was measured using Image J. To generate MK cells, mixed skin cells isolated from *Sirt7*$^{-/-}$, *Sirt7*-TG mice and WT littermates were plated in a collagen I/Fibronectin-coated dish and maintained in keratinocyte growth medium (KGM, Lonza, Swiss) with 15% FBS (Gibco), 20 ng/ml mouse recombinant VEGF-A, 20 ng/ml human recombinant FGF-2, 5 μM Y27632, and 50 μM $CaCl_2$.

Cell transfection and RNA interference

Plasmid and siRNA transfections were performed using Lipofectamine3000® (Thermo, USA), following the manufacturer's instructions. Custom siRNA oligos were synthesized by GenePharma (Shanghai, China). To obtain lentiviral particles, 10 μg lentiviral construct, 10 μg pSPAX2, and 5 μg pMD2G were co-transfected into HEK293T cells using Lipofectamine3000® (Thermo, USA). After ~ 48 h of transfection, the supernatants were collected and filtered through a 0.22-μm membrane (Merck, Germany). Virally infected cells were selected with 1 μg/ml puromycin (Merck, Germany) to obtain stable clones. The sequences of siRNAs used in this study are listed in Appendix Table S1.

NFATc1 activation assay

An NFAT-luc plasmid was purchased from Addgene (#17870, USA). To evaluate NFATc1 activity, NFAT-luc activity was measured using a Dual-luciferase reporter Assay System (Promega, USA). Briefly, HEK293T cells in a 24-well plate were transfected with 100 ng NFATc-luc, 25 ng pKL*4* Renilla luciferase control plasmid, and a SIRT7 construct using Lipofectamine 3000® (Thermo, USA). After 24 h, the cells were treated with 100 nM phorbol myristate acetate/2.5 μM ionomycin for an additional 4 h. Finally, NFATc1-luc activity was determined based on firefly luciferase activity normalized against Renilla luciferase, in accordance with the manufacturer's instructions.

RNA purification and real-time qPCR

Total RNA was isolated using TRIzol® reagent and RNAiso Plus (Takara, Japan). Total mRNA was reverse transcribed into cDNA using 5× Primescript® RT Master Mix (Takara). Quantitative real-time PCR was performed using 2× SYBR Green Mix (Takara) in a

Bio-Rad detection system. The primer sequences are provided in Appendix Table S1.

Plasmids

FLAG-NFATc1 and His-PA28γ were purchased from Vigenebio. CA-NFATc1 was purchased from Addgene (#11793). The SIRT7-related plasmids used were described in our previous study (Tang *et al*, 2017). NFATc1 lysine mutants were generated using a QuikChange Site-Directed Mutagenesis Kit (Stratagene). All constructs were verified by DNA sequencing (GENEWIZ, Guangzhou).

Protein extraction and immunoblotting

Protein extracts for immunoblotting were prepared in Laemmli loading buffer (0.1 M Tris–HCl (pH 7.0), 4% SDS, 20% glycerol, 1 mM DTT, and protease inhibitors); then, equal amounts of protein were separated by SDS–polyacrylamide gel electrophoresis and transferred to PVDF membranes (Millipore). The membranes were blocked for 1 h in 5% non-fat milk, and then incubated with primary antibodies in 3% BSA at 4°C overnight. After incubating with an HRP-coupled secondary antibody for 1 h, the immunoblots were visualized on a Bio-Rad system. The following antibodies were used in this research: SIRT7 (Santa Cruz, sc-365344, 1:3,000 dilution), NFATc1 (Abcam, ab2796, 1:1,000 dilution), β-catenin (CST, 8480, 1:1,000 dilution), active-β-catenin (CST, 19807, 1:1,000 dilution), PA28γ (CST, 2412, 1:1,000 dilution), SMDA1 (CST, 6944, 1:1,000 dilution), p-SMDA1 (CST, 13820, 1:1,000 dilution), Gli2 (CST, 2585S, 1:1,000 dilution), PTCH2 (CST, 2470, 1:1,000 dilution), SMAD2/3 (CST, 5678S, 1:1,000 dilution), pSMAD2(Ser465/467)/SMDA3(Ser423/425) (CST, 8828S, 1:1,000 dilution), CDK4 (Abcam, ab137675, 1:2,000), Pan acetyl-lysine (Abcam, ab21623, 1:500 dilution), Phospho-serine/threonine(p-S/T) (ECM Bioscience, PM3801, 1:2,000 dilution), H3K9ac (BioVision, 6872-25, 1:2,000 dilution), Msα His (ProteinTech, 66005-1-Ig, 1:5,000 dilution), HA-tag (Sigma-Aldrich, H3663, 1:5,000 dilution), Flag-tag (Sigma-Aldrich, F3165, 1:5,000 dilution), α-Tubulin (Beyotime, AT819, 1:5,000 dilution), and GAPDH (Beyotime, AG019, 1:5,000 dilution). Quantifications of the immunoblotting results were made using Image-Pro Plus 6.0.

Immunoprecipitation (IP)

Cells were first lysed in IP lysis buffer [150 mM NaCl, 25 mM Tris–HCl (pH 7.9), 5 mM $MgCl_2$, 10% glycerol, 0.2 mM EDTA, 0.1% NP-40, and protease inhibitors (Roche Complete)]. Cleared cell lysates were then incubated with antibodies or control IgGs coupled to 15 μl Protein A/G agarose beads (Invitrogen, USA) at 4°C for 4 h under rotation. The immunoprecipitates were washed, eluted in Laemmli loading buffer, and analyzed by immunoblotting.

GST pull-down assay

Cells were lysed in lysis buffer [120 mM KCl, 20 mM Tris–HCl (pH 7.9), 5 mM $MgCl_2$, 0.2 mM EDTA, 10% glycerol, 0.2% NP-40, and protease inhibitors (Roche Complete)], then incubated with 1 μg GST or GST-SIRT7 protein immobilized on Glutathione-Sepharose 4B (GE) at 4°C overnight. The beads were washed, eluted in Laemmli loading buffer, and then analyzed by immunoblotting.

LC-MS/MS analysis

Flag-NFATc1 transfected into HEK293T cells followed by NAM (MCE, HY-B0150) treatment was enriched using anti-Flag beads (Sigma-Aldrich) and separated by SDS-PAGE. After tryptic digestion, the peptides were subjected to NSI source followed by tandem mass spectrometry (MS/MS) in Q Exactive™ Plus (Thermo) coupled online to the UPLC. The peptides were then selected for MS/MS using the NCE setting as 28, and the fragments were detected in the Orbitrap at a resolution of 17,500. A data-dependent procedure was followed that alternated between one MS scan followed by 20 MS/MS scans with 15.0 s dynamic exclusion. Automatic gain control (AGC) was set at 5E4. The resulting MS/MS data were processed using Proteome Discoverer 1.3. Peptide confidence was set at high, and peptide ion score was set > 20.

Statistical analyses

The data represent the means ± s.e.m. Statistical differences were determined by Student's *t*-test using Prism or Microsoft Excel. A $P < 0.05$ was considered statistically significant.

Expanded View for this article is available online.

Acknowledgements
This study was supported by grants from the National Natural Science Foundation of China (91849208, 91749114, 81972602, 81702909, 81871114, 81773351, and 81601215), the National Key R&D Program of China (2017YFA0503900), the Science and Technology Program of Guangdong Province (2017B030301016, 2019B030301009), the Shenzhen Municipal Commission of Science and Technology Innovation (ZDSYS20190902093401689, KQJSCX20180328093403969, and JCYJ20180507182044945), and the SZU Medical Young Scientists Program. The authors would like to thank Dr. Jessica Tamanini (Shenzhen University and ETediting) for editing the manuscript prior to submission.

Author contributions
BL and JL supervised the work. BL, JL, and XT conceived the ideas of this project and wrote the manuscript. GL and XT performed the majority of the experiments. SZ and ZD helped to analyze hair cycle phenotypes. MJ helped to provide FACS analysis. ZL, MQ, MW, WS, ZW, and HX analyzed and discussed the results.

Conflict of interest
The authors declare that they have no conflict of interest.

References

Alonso L, Fuchs E (2003) Stem cells of the skin epithelium. *Proc Natl Acad Sci USA* 100(Suppl 1): 11830 – 11835

Andl T, Reddy ST, Gaddapara T, Millar SE (2002) WNT signals are required for the initiation of hair follicle development. *Dev Cell* 2: 643 – 653

Andl T, Ahn K, Kairo A, Chu EY, Wine-Lee L, Reddy ST, Croft NJ, Cebra-Thomas JA, Metzger D, Chambon P *et al* (2004) Epithelial Bmpr1a regulates differentiation and proliferation in postnatal hair follicles and is essential for tooth development. *Development* 131: 2257 – 2268

Araki S, Izumiya Y, Rokutanda T, Ianni A, Hanatani S, Kimura Y, Onoue Y, Senokuchi T, Yoshizawa T, Yasuda O *et al* (2015) Sirt7 contributes to myocardial tissue repair by maintaining transforming growth factor-beta signaling pathway. *Circulation* 132: 1081 – 1093

Bassino E, Vallariello E, Gasparri F, Munaron L (2017) Dermal-epidermal cross-talk: differential interactions with microvascular endothelial cells. *J Cell Physiol* 232: 897 – 903

Beals CR, Clipstone NA, Ho SN, Crabtree GR (1997a) Nuclear localization of NF-ATc by a calcineurin-dependent, cyclosporin-sensitive intramolecular interaction. *Genes Dev* 11: 824 – 834

Beals CR, Sheridan CM, Turck CW, Gardner P, Crabtree GR (1997b) Nuclear export of NF-ATc enhanced by glycogen synthase kinase-3. *Science* 275: 1930 – 1934

Blank MF, Grummt I (2017) The seven faces of SIRT7. *Transcription* 8: 67 – 74

Blanpain C, Lowry WE, Geoghegan A, Polak L, Fuchs E (2004) Self-renewal, multipotency, and the existence of two cell populations within an epithelial stem cell niche. *Cell* 118: 635 – 648

Botchkarev VA, Botchkareva NV, Nakamura M, Huber O, Funa K, Lauster R, Paus R, Gilchrest BA (2001) Noggin is required for induction of the hair follicle growth phase in postnatal skin. *FASEB J* 15: 2205 – 2214

Botchkarev VA, Botchkareva NV, Sharov AA, Funa K, Huber O, Gilchrest BA (2002) Modulation of BMP signaling by noggin is required for induction of the secondary (nontylotrich) hair follicles. *J Invest Dermatol* 118: 3 – 10

Botchkarev VA, Kishimoto J (2003) Molecular control of epithelial-mesenchymal interactions during hair follicle cycling. *J Investig Dermatol Symp Proc* 8: 46 – 55

Chai M, Jiang M, Vergnes L, Fu X, de Barros SC, Doan NB, Huang W, Chu J, Jiao J, Herschman H *et al* (2019) Stimulation of hair growth by small molecules that activate autophagy. *Cell Rep* 27: 3413 – 3421 e3413

Clipstone NA, Crabtree GR (1992) Identification of calcineurin as a key signalling enzyme in T-lymphocyte activation. *Nature* 357: 695 – 697

Cotsarelis G, Sun TT, Lavker RM (1990) Label-retaining cells reside in the bulge area of pilosebaceous unit: implications for follicular stem cells, hair cycle, and skin carcinogenesis. *Cell* 61: 1329 – 1337

Crabtree GR, Olson EN (2002) NFAT signaling: choreographing the social lives of cells. *Cell* 109(Suppl): S67 – S79

Ermolaeva M, Neri F, Ori A, Rudolph KL (2018) Cellular and epigenetic drivers of stem cell ageing. *Nat Rev Mol Cell Biol* 19: 594 – 610

Flanagan WM, Corthesy B, Bram RJ, Crabtree GR (1991) Nuclear association of a T-cell transcription factor blocked by FK-506 and cyclosporin A. *Nature* 352: 803 – 807

Foitzik K, Lindner G, Mueller-Roever S, Maurer M, Botchkareva N, Botchkarev V, Handjiski B, Metz M, Hibino T, Soma T *et al* (2000) Control of murine hair follicle regression (catagen) by TGF-beta1 *in vivo*. *FASEB J* 14: 752 – 760

Fujimura A, Michiue H, Nishiki T, Ohmori I, Wei FY, Matsui H, Tomizawa K (2011) Expression of a constitutively active calcineurin encoded by an intron-retaining mRNA in follicular keratinocytes. *PLoS ONE* 6: e17685

Gafter-Gvili A, Sredni B, Gal R, Gafter U, Kalechman Y (2003) Cyclosporin A-induced hair growth in mice is associated with inhibition of calcineurin-dependent activation of NFAT in follicular keratinocytes. *Am J Physiol Cell Physiol* 284: C1593 – C1603

Garcia-Rodriguez C, Rao A (1998) Nuclear factor of activated T cells (NFAT)-dependent transactivation regulated by the coactivators p300/CREB-binding protein (CBP). *J Exp Med* 187: 2031 – 2036

Goldstein J, Fletcher S, Roth E, Wu C, Chun A, Horsley V (2014) Calcineurin/Nfatc1 signaling links skin stem cell quiescence to hormonal signaling during pregnancy and lactation. *Genes Dev* 28: 983 – 994

Hogan PG, Chen L, Nardone J, Rao A (2003) Transcriptional regulation by calcium, calcineurin, and NFAT. *Genes Dev* 17: 2205 – 2232

Horsley V, Aliprantis AO, Polak L, Glimcher LH, Fuchs E (2008) NFATc1 balances quiescence and proliferation of skin stem cells. *Cell* 132: 299 – 310

Hsu YC, Pasolli HA, Fuchs E (2011) Dynamics between stem cells, niche, and progeny in the hair follicle. *Cell* 144: 92 – 105

Huelsken J, Vogel R, Erdmann B, Cotsarelis G, Birchmeier W (2001) beta-Catenin controls hair follicle morphogenesis and stem cell differentiation in the skin. *Cell* 105: 533 – 545

Jaks V, Barker N, Kasper M, van Es JH, Snippert HJ, Clevers H, Toftgard R (2008) Lgr5 marks cycling, yet long-lived, hair follicle stem cells. *Nat Genet* 40: 1291 – 1299

Kanfi Y, Naiman S, Amir G, Peshti V, Zinman G, Nahum L, Bar-Joseph Z, Cohen HY (2012) The sirtuin SIRT6 regulates lifespan in male mice. *Nature* 483: 218 – 221

Kawahara TL, Michishita E, Adler AS, Damian M, Berber E, Lin M, McCord RA, Ongaigui KC, Boxer LD, Chang HY *et al* (2009) SIRT6 links histone H3 lysine 9 deacetylation to NF-kappaB-dependent gene expression and organismal life span. *Cell* 136: 62 – 74

Keyes BE, Segal JP, Heller E, Lien WH, Chang CY, Guo X, Oristian DS, Zheng D, Fuchs E (2013) Nfatc1 orchestrates aging in hair follicle stem cells. *Proc Natl Acad Sci USA* 110: E4950 – E4959

Kim JH, Kim K, Youn BU, Jin HM, Kim JY, Moon JB, Ko A, Seo SB, Lee KY, Kim N (2011) RANKL induces NFATc1 acetylation and stability via histone acetyltransferases during osteoclast differentiation. *Biochem J* 436: 253 – 262

Kruglikov IL, Scherer PE (2016) Dermal adipocytes and hair cycling: is spatial heterogeneity a characteristic feature of the dermal adipose tissue depot? *Exp Dermatol* 25: 258 – 262

Kulessa H, Turk G, Hogan BL (2000) Inhibition of Bmp signaling affects growth and differentiation in the anagen hair follicle. *EMBO J* 19: 6664 – 6674

Lay K, Kume T, Fuchs E (2016) FOXC1 maintains the hair follicle stem cell niche and governs stem cell quiescence to preserve long-term tissue-regenerating potential. *Proc Natl Acad Sci USA* 113: E1506 – E1515

Lay K, Yuan S, Gur-Cohen S, Miao Y, Han T, Naik S, Pasolli HA, Larsen SB, Fuchs E (2018) Stem cells repurpose proliferation to contain a breach in their niche barrier. *Elife* 7: e41661

Lei M, Chuong CM (2016) STEM CELLS. Aging, alopecia, and stem cells. *Science* 351: 559 – 560

Li J, Gao X, Ortega J, Nazif T, Joss L, Bogyo M, Steven AC, Rechsteiner M (2001) Lysine 188 substitutions convert the pattern of proteasome activation by REGgamma to that of REGs alpha and beta. *EMBO J* 20: 3359 – 3369

Li L, Zhao D, Wei H, Yao L, Dang Y, Amjad A, Xu J, Liu J, Guo L, Li D *et al* (2013) REGgamma deficiency promotes premature aging via the casein kinase 1 pathway. *Proc Natl Acad Sci USA* 110: 11005 – 11010

Li L, Shi L, Yang S, Yan R, Zhang D, Yang J, He L, Li W, Yi X, Sun L *et al* (2016) SIRT7 is a histone desuccinylase that functionally links to chromatin compaction and genome stability. *Nat Commun* 7: 12235

Mao I, Liu J, Li X, Luo H (2008) REGgamma, a proteasome activator and beyond? *Cell Mol Life Sci* 65: 3971 – 3980

Matsumura H, Mohri Y, Binh NT, Morinaga H, Fukuda M, Ito M, Kurata S, Hoeijmakers J, Nishimura EK (2016) Hair follicle aging is driven by transepidermal elimination of stem cells via COL17A1 proteolysis. *Science* 351: aad4395

Millar SE (2002) Molecular mechanisms regulating hair follicle development. *J Invest Dermatol* 118: 216 – 225

Mohrin M, Shin J, Liu Y, Brown K, Luo H, Xi Y, Haynes CM, Chen D (2015) Stem cell aging. A mitochondrial UPR-mediated metabolic checkpoint regulates hematopoietic stem cell aging. *Science* 347: 1374 – 1377

Morris RJ, Liu Y, Marles L, Yang Z, Trempus C, Li S, Lin JS, Sawicki JA, Cotsarelis G (2004) Capturing and profiling adult hair follicle stem cells. *Nat Biotechnol* 22: 411 – 417

Muller-Rover S, Handjiski B, van der Veen C, Eichmuller S, Foitzik K, McKay IA, Stenn KS, Paus R (2001) A comprehensive guide for the accurate classification of murine hair follicles in distinct hair cycle stages. *J Invest Dermatol* 117: 3 – 15

Neal JW, Clipstone NA (2001) Glycogen synthase kinase-3 inhibits the DNA binding activity of NFATc. *J Biol Chem* 276: 3666 – 3673

Neal JW, Clipstone NA (2003) A constitutively active NFATc1 mutant induces a transformed phenotype in 3T3-L1 fibroblasts. *J Biol Chem* 278: 17246 – 17254

O'Callaghan C, Vassilopoulos A (2017) Sirtuins at the crossroads of stemness, aging, and cancer. *Aging Cell* 16: 1208 – 1218

Oshimori N, Fuchs E (2012) Paracrine TGF-beta signaling counterbalances BMP-mediated repression in hair follicle stem cell activation. *Cell Stem Cell* 10: 63 – 75

Plasari G, Edelmann S, Hogger F, Dusserre Y, Mermod N, Calabrese A (2010) Nuclear factor I-C regulates TGF-{beta}-dependent hair follicle cycling. *J Biol Chem* 285: 34115 – 34125

Porter CM, Havens MA, Clipstone NA (2000) Identification of amino acid residues and protein kinases involved in the regulation of NFATc subcellular localization. *J Biol Chem* 275: 3543 – 3551

Realini C, Jensen CC, Zhang Z, Johnston SC, Knowlton JR, Hill CP, Rechsteiner M (1997) Characterization of recombinant REGalpha, REGbeta, and REGgamma proteasome activators. *J Biol Chem* 272: 25483 – 25492

Reddy S, Andl T, Bagasra A, Lu MM, Epstein DJ, Morrisey EE, Millar SE (2001) Characterization of Wnt gene expression in developing and postnatal hair follicles and identification of Wnt5a as a target of Sonic hedgehog in hair follicle morphogenesis. *Mech Dev* 107: 69 – 82

Reichenbach B, Classon J, Aida T, Tanaka K, Genander M, Goritz C (2018) Glutamate transporter Slc1a3 mediates inter-niche stem cell activation during skin growth. *EMBO J* 37: e98280

Rishikaysh P, Dev K, Diaz D, Qureshi WM, Filip S, Mokry J (2014) Signaling involved in hair follicle morphogenesis and development. *Int J Mol Sci* 15: 1647 – 1670

Ryu D, Jo YS, Lo Sasso G, Stein S, Zhang H, Perino A, Lee JU, Zeviani M, Romand R, Hottiger MO *et al* (2014) A SIRT7-dependent acetylation switch of GABPbeta1 controls mitochondrial function. *Cell Metab* 20: 856 – 869

Samuelov L, Sprecher E, Tsuruta D, Biro T, Kloepper JE, Paus R (2012) P-cadherin regulates human hair growth and cycling via canonical Wnt signaling and transforming growth factor-beta2. *J Invest Dermatol* 132: 2332 – 2341

Sato N, Leopold PL, Crystal RG (1999) Induction of the hair growth phase in postnatal mice by localized transient expression of Sonic hedgehog. *J Clin Invest* 104: 855 – 864

Satoh A, Brace CS, Rensing N, Cliften P, Wozniak DF, Herzog ED, Yamada KA, Imai S (2013) Sirt1 extends life span and delays aging in mice through the regulation of Nk2 homeobox 1 in the DMH and LH. *Cell Metab* 18: 416 – 430

Schmidt-Ullrich R, Paus R (2005) Molecular principles of hair follicle induction and morphogenesis. *BioEssays* 27: 247 – 261

Shin J, He M, Liu Y, Paredes S, Villanova L, Brown K, Qiu X, Nabavi N, Mohrin M, Wojnoonski K *et al* (2013) SIRT7 represses Myc activity to suppress ER stress and prevent fatty liver disease. *Cell Rep* 5: 654 – 665

Stenn KS, Paus R (2001) Controls of hair follicle cycling. *Physiol Rev* 81: 449 – 494

Tang BL (2015) SIRT7 and hepatic lipid metabolism. *Front Cell Dev Biol* 3: 1

Tang X, Shi L, Xie N, Liu Z, Qian M, Meng F, Xu Q, Zhou M, Cao X, Zhu WG *et al* (2017) SIRT7 antagonizes TGF-beta signaling and inhibits breast cancer metastasis. *Nat Commun* 8: 318

Tang M, Li Z, Zhang C, Lu X, Tu B, Cao Z, Li Y, Chen Y, Jiang L, Wang H *et al* (2019) SIRT7-mediated ATM deacetylation is essential for its deactivation and DNA damage repair. *Sci Adv* 5: eaav1118

Tang X, Li G, Su F, Cai Y, Shi L, Meng Y, Liu Z, Sun J, Wang M, Qian M *et al* (2020) HDAC8 cooperates with SMAD3/4 complex to suppress SIRT7 and promote cell survival and migration. *Nucleic Acids Res* 48: 2912 – 2923

Tumbar T, Guasch G, Greco V, Blanpain C, Lowry WE, Rendl M, Fuchs E (2004) Defining the epithelial stem cell niche in skin. *Science* 303: 359 – 363

Vakhrusheva O, Smolka C, Gajawada P, Kostin S, Boettger T, Kubin T, Braun T, Bober E (2008) Sirt7 increases stress resistance of cardiomyocytes and prevents apoptosis and inflammatory cardiomyopathy in mice. *Circ Res* 102: 703 – 710

Vazquez BN, Thackray JK, Simonet NG, Kane-Goldsmith N, Martinez-Redondo P, Nguyen T, Bunting S, Vaquero A, Tischfield JA, Serrano L (2016) SIRT7 promotes genome integrity and modulates non-homologous end joining DNA repair. *EMBO J* 35: 1488 – 1503

Wang L, Siegenthaler JA, Dowell RD, Yi R (2016) Foxc1 reinforces quiescence in self-renewing hair follicle stem cells. *Science* 351: 613 – 617

Wilk S, Chen WE, Magnusson RP (2000) Properties of the nuclear proteasome activator PA28gamma (REGgamma). *Arch Biochem Biophys* 383: 265 – 271

Wu D, Li Y, Zhu KS, Wang H, Zhu WG (2018) Advances in cellular characterization of the sirtuin isoform, SIRT7. *Front Endocrinol (Lausanne)* 9: 652

Yoshizawa T, Karim MF, Sato Y, Senokuchi T, Miyata K, Fukuda T, Go C, Tasaki M, Uchimura K, Kadomatsu T *et al* (2014) SIRT7 controls hepatic lipid metabolism by regulating the ubiquitin-proteasome pathway. *Cell Metab* 19: 712 – 721

Zhang J, He XC, Tong WG, Johnson T, Wiedemann LM, Mishina Y, Feng JQ, Li L (2006) Bone morphogenetic protein signaling inhibits hair follicle anagen induction by restricting epithelial stem/progenitor cell activation and expansion. *Stem Cells* 24: 2826 – 2839